# Journal of Materials Chemistry C

Accepted Manuscript


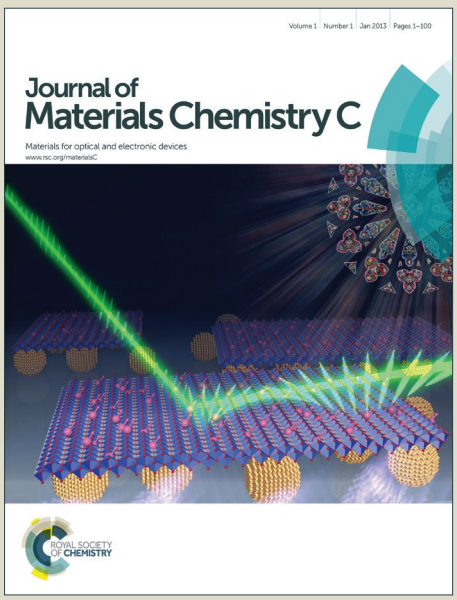





ROYAL SOCIETY OF CHEMISTRY

www.rsc.org/materialsC

Journal of
Materials Chemistry C

REVIEW ARTICLE

# Recent development in phosphors with different emitting colors via energy transfer for FEDs and UV/n-UV w-LEDs

Received 00th January 20xx,
Accepted 00th January 20xx

DOI: 10.1039/x0xx00000x

www.rsc.org/

Kai Li[ab], Mengmeng Shang[a], Hongzhou Lian[a] and Jun Lin*[a]

Utilizing energy transfer (ET) between the sensitizer and acceptor in phosphors is a good way to obtain tunable emission color. Therefore, many researchers have devoted their interest to design the phosphors samples with different emission colors via energy transfer properties. It is well known that $Ce^{3+}$ and $Bi^{3+}$ are the good sensitizers, while the $Mn^{2+}$, $Dy^{3+}$, $Eu^{3+}$ and $Sm^{3+}$ can be the useful activators. And $Eu^{2+}$ and $Tb^{3+}$ can be both good sensitizers and activators. Therefore, herein we summary many recent ET systems consisting of $Eu^{2+}$-$Mn^{2+}$/$Tb^{3+}$, $Eu^{2+}$-$Tb^{3+}$-$Mn^{2+}$/$Eu^{3+}$/$Sm^{3+}$, $Ce^{3+}$-$Mn^{2+}$/$Tb^{3+}$/$Dy^{3+}$/$Eu^{2+}$, $Ce^{3+}$-$Tb^{3+}$-$Mn^{2+}$/$Eu^{3+}$/$Sm^{3+}$, $Bi^{3+}$-$Eu^{3+}$/$Sm^{3+}$ and $Tb^{3+}$-$Eu^{3+}$/$Sm^{3+}$ in this article, which show the tunable emission color from ultraviolet to blue and green, blue to green, yellow, orange and pink/red, cyan to green, orange and pink/red, and green to yellow/orange and red. Based on this, this review would be a good reference to benefit the design and investigation of phosphors potentially applied in FEDs and LEDs with ET in them.

## 1. Introduction

In the past decades, the utilization of inorganic phosphor materials gives a fast growing development due to their broad aspects of applications, such as cathode ray tubes (CRTs), light-emitting diodes (LEDs), field-emission displays (FEDs), vacuum fluorescent displays (VFDs), plasma display panels (PDPs).[1] The global issues of energy saving and environmental protection inspire the substitution of white-LEDs (w-LEDs) for conventional fluorescent and incandescent lamps, which is ascribed to its special merits such as high efficiency, long operation lifetime, portal compactness and etc. besides energy saving and non-pollution.[2] Moreover, in the display field, the FEDs is considered to be a well potential candidate for liquid crystal displays (LCDs) currently applied in the mart because of their many superiorities on viewing, lighting, power depletion, operated-temperature range, response time, and so on.[3] Therefore, the attention focused on them is especially increasing all the time. Nowadays, there mainly exist two methods to obtain white light in LEDs, eg., commercial way is combining a blue chip with YAG:$Ce^{3+}$ phosphors, the other is employing different color-emitting LEDs (blue+green+red LEDs).[4] However, the deficiency of former is lacking of red component, which results in the poor color rendering indices (CRI < 80) and a high correlated color temperature (CCT > 4500 K), restricting the vivid application for indoor lighting in the future.[5] As to later one, many practical problems should be considered, such as different driving voltage, lighting output, temperature characteristic, lighting decay velocity, working lifetime, fabrication price and etc. for different color-emitting LEDs. To improve and avoid these issues, another alternative two routes involving the employments of ultraviolet/near-ultraviolet (UV/n-UV) LEDs with blue, green and red phosphors or singly-phased white light-emitting phosphors are advocated to generate w-LEDs in recent years.[6] Generally, to build highly efficient w-LED devices, three related factors including semiconducting components (general $Al_{1-x}Ga_xN$ semiconductor chips), phosphor components and packaging technologies, should be considered and optimized. As the indispensable components of w-LED devices, phosphors with different emission colors are being explored and developed for use in lighting and display backlight sources, which is considered to be one of the most critical and urgent challenges in lighting field. It is well known the $Eu^{2+}$, $Ce^{3+}$ and $Bi^{3+}$ can emit broad bands with different colors in various hosts based on their $4f^6 5d^1$-$4f^7$, $5d^1$-$4f^1$ and $^3P_1$-$^1S_0$ allowed transitions,[7] respectively, and different crystal fields around them. Therefore, the tuning of emission color can be realized in $Eu^{2+}$, $Ce^{3+}$ and $Bi^{3+}$ singly doped phosphors by ions substitution methods, which have been presented in recent review by Li et al.[8] and paper by Kang et al.[9] However, $Eu^{2+}$, $Ce^{3+}$ and $Bi^{3+}$ also can be served as efficient sensitizers to transfer their energy to activators such as $Mn^{2+}$, $Tb^{3+}$, $Dy^{3+}$, $Eu^{3+}$ and $Sm^{3+}$ to produce abundant and tunable emission colors including white via adjusting doped ions concentrations.[10] Sometime, $Tb^{3+}$ also can be an effieient sensitizer to transfer its energy to $Eu^{3+}$ or $Sm^{3+}$ to obtain the tunable emission color from green to orange/red under UV excitation.[11] Therefore, it is a good way to control and adjust the emission colors of phosphors via utilizing the ET properties between doped ions. Table 1 summaries the transitional characteristics of singly-doped ions in phosphors mentioned above, which is useful for us to interpret the photoluminescence features of them.

As mentioned above, ET, a good strategy to control the emission color, has been extensively utilized in phosphors.[39] Fig. 1a simply

[a]State Key Laboratory of Rare Earth Resource Utilization, Changchun Institute of Applied Chemistry, Chinese Academy of Sciences, Changchun 130022, P. R. China. Email: jlin@ciac.ac.cn (Jun Lin); Fax: +86-431 - 85698041; TEL: 86-431-85262031
[b]University of Chinese Academy of Sciences, Beijing 100049, P. R. China.

describes the energy migration process in luminescence materials. Sometimes, the exciting energy can not or little be absorbed by the activator (A), therefore, another ion (S) was added into the host lattice to absorb exciting radiation and subsequently transfer its energy to the activator, then the emission was produced. This process can be expressed with a simple expression analogous to a chemical reaction S* + A → S + A* (Fig. 1b), where the asterisk represents the excited state of doped ions. The excited state A* has two ways to fall to ground state A, one is radiation transition method (lighting), the other is non-radiate transition route (quenching). In former case, the S is called a sensitizer of A, while in later one, the A is said to be a quencher of S. ET between two centers requires a certain interaction between them. Considering two centers, S and A, separate in a solid by distance R, if the R is so short that the center S and A have a non-vanishing interaction with each other. Therefore, the relaxed excited state S* may transfer its energy to A. The rate of this ET process had been calculated by Forster before, after whom Dexter extended this treatment to other interaction types.[40] In general, resonant ET is dominant in the generation of up-conversion (UC) and down-conversion (DC) in most rare-earth (RE) doped phosphors systems. It can only occur if the energy gap between ground and excited state of S and A is equal, as well as a suitable interaction between S and A (Fig. 1c). The interaction types include an exchange interaction (if it has the wave function overlap) and an electric or magnetic multipolar interactions. The ET rate had been proposed by considering the spectral overlap between the emission spectrum of S and absorption spectrum of A with following equation:[41]

$$P_{SA} = \frac{2\pi}{\hbar}\left|< S, A^* \left| H_{SA} \right| S^*, A >\right|^2 \cdot \int g_s(E) g_A(E)\, dE \quad (1)$$

Where the integral represents the spectral overlap, $g_s(x)$ is the normalized line shape function of center x, where it is hatched in Fig. 1d, $H_{SA}$ is the interaction Hamiltonian, the matrix element is the interaction between the original state | S*,A> and the final state | S,A*>. If the ET process from S to A occurs, the rate $P_{SA}$ should not be zero, therefore, neither term $\left|< S, A^* \left| H_{SA} \right| S^*, A >\right|^2$ nor $\int g_s(E) g_A(E)\, dE$ is zero, which means (1) the emission band of S should spectrally overlap the excitation band of A, (2) the S and A need to be interacted with each other including the electric multipole-multipole interactions type or exchange interaction. The transitional intensity determines the strength of electric multipole interactions. High ET rate can be only anticipated if the transition processes concerned are allowed electric dipole transitions. Although the disappreance of absorption intensity results in the disappearance of electric multipole interaction, the transfer rate may not vanish because exchange interaction can contribute to it. The exchange interaction depends on the wave function overlap, which decays exponentially to the distance of R. While for electric multipole interactions, the distance dependence is given by $R^{-n}$, in which n = 6, 8, 10 corresponds to electric dipole-dipole, dipole-quadrupole, quadrupole-quadrupole interactions. The excited state S* can not only decay to ground themselves with a rate $P_S$ (radiate rate) but also transfer its energy to A with a rate $P_{SA}$. The critical distance ($R_c$) is defined when the $P_S$ equals to $P_{SA}$, that is to say, if the distance between S and A equals to $R_c$, the radiate rate equals to ET rate. Therefore, the radiate transition of S prevails for $R>R_c$ while the ET from S to A is dominant for $R<R_c$. If the ET occurs in a system, the fluorescent decay lifetimes of sensitizer should decline with the increase of activator content, the decay curves may be fitted with single, double, especially three exponential functions,[42] which are expressed below:

$$I(t) = I_0 + A_1 \exp\left(-\frac{t}{\tau_2}\right) + \cdots A_n \exp\left(-\frac{t}{\tau_n}\right) \quad (2)$$

$$\tau = \left(A_1\tau_1^2 + \cdots A_n\tau_n^2\right) \Big/ \left(A_1\tau_1 + \cdots A_n\tau_n\right) \quad (3)$$

n = 1, 2 and 3 correspond to single, double and three exponential functions, respectively. Sometimes, none of the exponential decay function is proper with the decay curves, the effective lifetime should be defined as follow:[43]

$$\tau = \frac{\int_0^\infty tI(t)\,dt}{\int_0^\infty I(t)\,dt} \quad (4)$$

$$\tau = \int_0^\infty I(t)dt \quad (5)$$

$t$ is the time with the decay of fluorescent intensity; $\tau$ is the fluorescent decay lifetime.

In order to determine the ET mechanism from sensitizers to activators, the ET formula of exchange interaction and electric multipolar interactions proposed by Dexter's and Reisfeld's was utilized:[44]

$$\eta_{S0}/\eta_S \propto C^{n/3} \quad (6)$$

in which $\eta_{S0}$ is the intrinsic luminescence quantum efficiency of the sensitizer; $\eta_S$ is the luminescence quantum efficiency of the sensitizer with the existence of activator; and $C$ is the sum of dopant ion concentration. The n = 3, 6, 8 and 10 correspond to exchange interaction, electric dipole-dipole, dipole-quadrupole and quadrupole-quadrupole interactions, respectively. However, the value of $\eta_{S0}/\eta_S$ is hard to be acquired, therefore, it can be replaced approximately from the correlated intensity ($I_{S0}/I_S$) or lifetime ratio ($\tau_{S0}/\tau_S$):[45]

$$I_{S0}/I_S \propto C^{n/3} \text{ or } \tau_{S0}/\tau_S \propto C^{n/3} \quad (7)$$

By examinating the linear fitting factor $R^2$ of the relationship above, the biggest $R^2$ indicates the corresponding ET mechanism. Sometimes, the Inokuti-Hirayama (I-H) model is also applied to analyze the ET mechanism through fluorescent decay curves, which is satisfactory to describe ET processes if the donor-acceptor transfer is much faster than the diffusion among the donors. As to electric multipolar interactions, the following equation can depict the time evolution of the emission from the donor:[46]

$$I(t) = I_0 \exp\left[-\frac{t}{\tau_0} - \alpha\left(\frac{t}{\tau_0}\right)^{3/S}\right] \quad (8)$$

where $I(t)$ corresponds to the emission intensity after pulsed excitation, $I_0$ refers to the emission intensity at $t$ = 0, $\tau_0$ is the intrinsic decay time of the donor ion, α is a parameter involving the ET probability, and $S$ is an indication of the electric multipolar interactions character; $S$ = 6, 8 and 10 for electric dipole-dipole, dipole-quadrupole and quadrupole-quadrupole interactions,



 

respectively. After modification, the expression can be depicted as follow:

$$In\left[-In\frac{I(t)}{I_0}-\left(\frac{t}{\tau_0}\right)\right]\propto In\left(\frac{t}{\tau_0}\right)^{3/S} \quad (9)$$

After plotting the curves according to the equation above, a fitting straight line will be yielded with the slope equal to 3/*S*. Therefore, the *S* can be determined. To certify the correction of ET mechanism deduced by two methods above, the ET $R_c$ calculated via concentration quenching and spectral overlap methods should be identical. The $R_c$ is calculated using follow formula:[47]

$$R_c = 2\left(\frac{3V}{4\pi x_c N}\right)^{1/3} \quad (10)$$

In the formula, *V* is the volume of the unit cell, *N* is the number of cations in the unit cell of the host, $x_c$ is the sum of donor and acceptor concentrations, at which the emission intensity of the donor in the presence of the acceptor is half that in the absence of the acceptor. Since the values of parameters can be readily obtained , the $R_c$ can be determined. As for dipole-dipole and dipole-quadrupole interactions, the $R_c$ can be calculated approximately using spectral overlap method, which are expressed below:[48]

$$R_c^6 = 3.024\times10^{12} f_d \int \frac{f_S(E)F_A(E)}{E^4}dE \quad (11)$$

$$R_c^8 = 3.024\times10^{12} \lambda_S^2 f_q \int \frac{f_S(E)F_A(E)}{E^4}dE \quad (12)$$

where $f_d$ and $f_q$ refer to the oscillator intensities of the transition absorption for the activator, $R_c$ represents the distance between the activator and the sensitizer, *E* is the energy (in eV)involved in the transfer process, $\int f_S(E)f_A(E)/E^4\,dE$ refers to the spectral overlap between the normalized shapes of the emission $f_S$(E) from sensitizer and the excitation $f_A$(E) from activator, $\lambda_S$ (in angstroms) is the wavelength position of the sensitizer's emission. Accordingly, the $R_c$ are evaluated after the acquirement of parameters above. Commonly, the $R_c$ calculated by two ways can be close to each other, which illustrates the correction of the discussion of ET mechanism between doped ions in phosphors.

Recently, Liu et al.[49a] reviewed the ET in bulk and nanoscale luminescence materials involving metal ions, quantum dots (QDs), organic species, 2D materials and plasmonic nanostructures. Shinde et al.[49b] reviewed the europium-activated orthophosphate phosphors for solid lighting, they discussed the synthesis of a family of orthophosphate phosphor doped with europium ($Eu^{2+}$ and $Eu^{3+}$) by traditional and novel methods. Shang et al.[49c] summarized the methods to realize the single-phase white-light-emitting in materials. However, the detailed ET in phosphors is rarely discussed. In this review paper, we focus on the recent development of various phosphors systems potentially applied in FEDs and LEDs with ET in detail because the topic themed has aroused extensive research interest in recent years. Moreover, the overview of luminescence characteristic of doped ions in phosphors can be understood to guide the design and investigation of phosphors with ET in them.

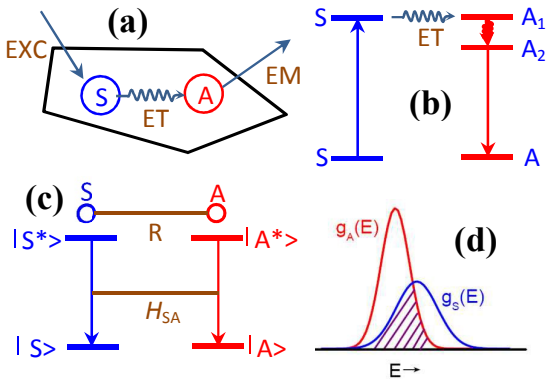


**Fig. 1** (a) ET from a sensitizer S to an activator A. (b) Energy levels diagram of ET from S to A, the S→S* is the absorption, $A_2$*→A is the emission, $A_1$*→$A_2$* is the non-radiative decay. (c) The two centers are at a distance of R, the energy level schemes and interaction $H_{SA}$ are given. (d) The spectral overlap of excitation spectrum of A and emission spectrum of S.

## 2. Phosphors systems with different emitting colours via energy transfer

### 2.1 $Eu^{2+}$-$Mn^{2+}$/$Tb^{3+}$ systems

A large amount of $Eu^{2+}$ singly-doped phosphors have been reported recently.[12-17] The emission color can be varied from blue to red in different hosts, which are represented in Table 1. However, the emission color is generally unchangeable or little changeable in certain systems. In order to tune the emission color and obtain abundant colors, the energy transfer properties from $Eu^{2+}$ to $Mn^{2+}$/$Tb^{3+}$ are frequently utilized in phosphors. The emission color can be tuned from blue to green, yellow, orange and even pink/red, cyan to pink and green to yellow, orange and pink/red for $Eu^{2+}$-$Mn^{2+}$ system, and from blue or cyan to green for $Eu^{2+}$-$Tb^{3+}$ system.

$Eu^{2+}$-$Mn^{2+}$ system is one of the most abundant systems for the emission color adjustment in phosphors. $Mn^{2+}$, a transitional-metal element, can emit different colors from green (tetrahedron field) to red (octahedron field) originated from the different crystal fields $Mn^{2+}$ around, as listed in Table 1. Moreover, its excitation bands often locate in blue and green areas. Therefore, blue or green emission spectra of $Eu^{2+}$ may overlap the excitation spectra of $Mn^{2+}$, which may generate the ET from $Eu^{2+}$ to $Mn^{2+}$ and result in tunable color under appropriate excitation in some hosts. Liu et al.[50] synthesized a novel blue to green phosphor γ-AlON:$Eu^{2+}$,$Mn^{2+}$ at 1800 °C under 0.5 MPa $N_2$ by using the gas-pressure sintering method (GPS). They found $Eu^{2+}$ singly-doped γ-AlON can emit a wide band centered at 470 nm corresponding to the blue color with the excitation band from 200 to 450 nm, and $Mn^{2+}$ singly-doped γ-AlON can produce a broad band peaking at 517 nm under 450 nm excitation. Both of them were considered to occupy $Al^{3+}$ sites, however, the mismatch of ionic radii $Al^{3+}$ (0.39 Å, 4CN) and $Eu^{2+}$ (1.17 Å, 4CN) limited the solubility of $Eu^{2+}$ (Fig. 2a). Spectral overlap between $Eu^{2+}$ emission and $Mn^{2+}$ excitation was presented in the paper, which gave a possibility of ET from $Eu^{2+}$ to $Mn^{2+}$ ions in $Eu^{2+}$,$Mn^{2+}$ co-doped samples. Moreover, the similar excitation spectra of $Eu^{2+}$ and $Mn^{2+}$ emissions in $Eu^{2+}$,$Mn^{2+}$ co-doped samples were used to demonstrate it. Therefore, the emission intensity of $Mn^{2+}$ can be enhanced by many times compared to $Mn^{2+}$ singly-

**Table 1** The transitional character of singly-doped ions in phosphors

| Doped ions category | Main energy levels transition | Representative samples | Emission colors | Ref. |
|---|---|---|---|---|
| $Eu^{2+}$ | $4f^65d^1 \rightarrow 4f^7$ | $Ca_3Mg_3(PO_4)_4:Eu^{2+}$ | blue | 12 |
| | | $Ca_3(PO_4)_2:Eu^{2+}$ | cyan | 13 |
| | | $CaZrSi_2O_7:Eu^{2+}$ | green | 14 |
| | | $Ca_3Si_2O_7:Eu^{2+}$ | yellow | 15 |
| | | α-$SrNCN:Eu^{2+}$ | orange | 16 |
| | | $Sr[LiAl_3N_4]:Eu^{2+}$ | red | 17 |
| $Ce^{3+}$ | $5d^1 \rightarrow 4f^1$ | $Sr_5(PO_4)_2(SiO_4):Ce^{3+}$ | blue | 18 |
| | | $Ca_6BaP_4O_{17}:Ce^{3+}$ | Blue-green | 19 |
| | | $Ca_2GdZr_2(AlO_4)_3:Ce^{3+}$ | green | 20 |
| | | $(La,Gd)Sr_2(Al,B)O_5:Ce^{3+}$ | yellow | 21 |
| | | $Y_3Al_{5-x}Si_xO_{12-x}N_x:Ce^{3+}$ | orange | 22 |
| | | $SrS:Ce^{3+}$ | red | 23 |
| $Bi^{3+}$ | $^3P_1 \rightarrow {}^1S_0$ | $CaSb_2O_6:Bi^{3+}$ | blue | 24 |
| | | $Ca_{12}Al_{14}O_{32}Cl_2:xBi^{3+}$ | cyan | 25 |
| | | $Ca_3Al_2O_6$: $Bi^{3+}$ | green | 26 |
| | | $LuVO_4:Bi^{3+}$ | yellow | 27 |
| | | $ScVO_4:Bi^{3+}$ | orange | 28 |
| $Mn^{2+}$ | $^4T_1 \rightarrow {}^6A_1$ | $NaZnPO_4:Mn^{2+}$ | green | 29 |
| | | $CdSiO_3:Mn^{2+}$ | yellowish orange | 30 |
| | | $Na_2CaMg(PO_4)_2:Mn^{2+}$ | red | 31 |
| $Tb^{3+}$ | $^5D_4 \rightarrow {}^7F_{J(J=6,5,4,3)}$ | $CaMoO_4:Tb^{3+}$ | green | 32 |
| $Dy^{3+}$ | $^4F_{9/2} \rightarrow {}^6H_{15/2}$ $^4F_{9/2} \rightarrow {}^6H_{13/2}$ | $Sr_3RE_2(BO_3)_4:Dy^{3+}$ (RE = Y, La, Gd) | cyan | 33 |
| | | $(Sr_{0.85}Mg_{0.14})_3(P_{1-x}Si_xO_4)_2:Dy^{3+}$ | white | 34 |
| | | $Y_2(MoO_4)_3:Dy^{3+}$ | yellow | 35 |
| $Sm^{3+}$ | $^4G_{5/2} \rightarrow {}^6H_{5/2,7/2,9/2}$ | $SrMoO_4:Sm^{3+}$ | red | 36 |
| $Eu^{3+}$ | $^5D_0 \rightarrow {}^7F_{J(J=0,1,2,3,4)}$ | $Ba_2CaWO_6$: $Eu^{3+}$ | orange red | 37 |
| | | $RbZnPO_4:Eu^{3+}$ | red | 38 |

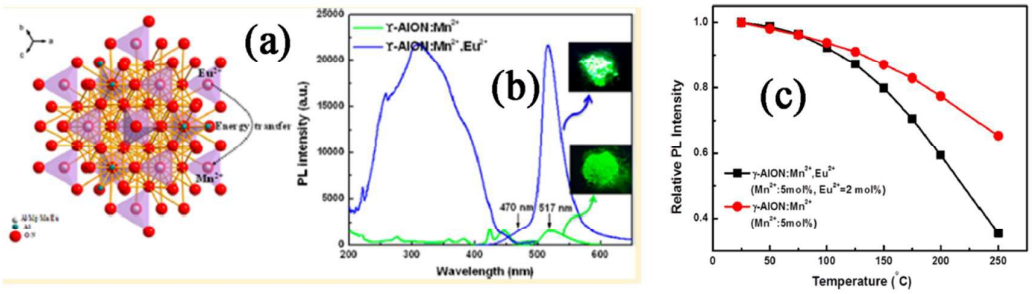


**Fig. 2** (a) Site occupation of $Eu^{2+}$ and $Mn^{2+}$ in crystal structure of γ-AlON and comparison of photoluminescence (PL) spectra of γ-AlON:$Eu^{2+}$ (blue), γ-AlON:$Mn^{2+}$ (red), and γ-AlON:$Mn^{2+}$,$Eu^{2+}$ (green). (b) Temperature-dependent luminescence of γ-AlON:$Eu^{2+}$,$Mn^{2+}$ ($Eu^{2+}$ = 2 mol %, $Mn^{2+}$ = 5 mol %) and γ-AlON:$Mn^{2+}$($Mn^{2+}$ = 5 mol %). Excitation wavelength is 405 nm. (Reproduced with permission from ref. 50 copyright 2015, American Chemical Society.)

doped situation (Fig. 2b). Good thermal stability was deduced because the emission intensity of γ-AlON:$Eu^{2+}$,$Mn^{2+}$ measured at 150 °C maintained 80% of that at room temperature (Fig. 2c), which was 8% larger than that of γ-AlON:$Mn^{2+}$. This may be originated from a serious lattice distortion when $Eu^{2+}$ and $Mn^{2+}$ were co-doped into γ-AlON with appreciable difference ionic radii. As to $Ca_9Mg(PO_4)_6F_2:Eu^{2+},Mn^{2+}$ system,[51] the new solid solution of $Ca_9Mg(PO_4)_6F_2$ was obtained via a substitution of Mg for Ca with the similar crystal structure of $Ca_5(PO_4)_3F$. As is well known to us, the $Ca_5(PO_4)_3F$ belongs to the apatite hexagonal structure with a space group $P_{63/m}$, in which there are two kinds of crystallographic lattices consisting of 9-fold-coordinated 4f sites with $C_3$ point symmetry [denoted as $Ca^{2+}(1)$] and 7- fold-coordinated 6h sites with $C_s$ point symmetry [denoted as $Ca^{2+}(2)$] (Fig. 3a). Therefore, $Eu^{2+}$ would like to occupy both two sites, resulting in an asymmetrically broad band and it can be decomposed into two Gaussian bands (Fig. 3b), which was demonstrated by the different fluorescent decay lifetimes for two deconvoulted bands (Fig. 3c). Intense tunable emission color from blue to yellow including white along with the CIE chromatic coordinates was observed under a 365 nm UV lamp excitation in $Eu^{2+}$,$Mn^{2+}$ co-doped $Ca_9Mg(PO_4)_6F_2$ by adjusting the ratio of $Eu^{2+}$

and $Mn^{2+}$ concentrations (Fig. 3d). This phenomenon is based on the ET from $Eu^{2+}$ to $Mn^{2+}$ ions, which was also demonstrated by the similar excitation spectra of $Eu^{2+}$ and $Mn^{2+}$ and decline of fluorescent decay lifetimes of $Eu^{2+}$ (Fig. 3e) in $Ca_9Mg(PO_4)_6F_2:Eu^{2+},Mn^{2+}$. When four Ca atoms were substituted by two Y and two Na atoms to balance the charge in $Ca_{10}(PO_4)_6F_2$, the similar phenomenon was also presented and observed in apatite crystal structure phosphor $Ca_6Y_2Na_2(PO_4)_6F_2:Eu^{2+},Mn^{2+}$.[52] The substitution of all Ca atoms by Sr atoms in this kind of crystal structure also can produce the tunable emission color from blue to yellow in $Sr_5(PO_4)_3F:Eu^{2+},Mn^{2+}$.[53] Another good blue-white-yellow system $Ca_2YF_4(PO_4):Eu^{2+},Mn^{2+}$ was also investigated by Geng et al.[54] Huang et al.[55] successfully combined the as-prepared $Ca_4Si_2O_7F_2:Eu^{2+},Mn^{2+}$ phosphors with a 400 nm n-UV chip to fabricate a w-LED, producing a good CIE chromatic coordinate of (0.347,0.338) and CCT of 4880 K compared to commercial w-LED with the CIE chromatic coordinate of (0.302,0.315) and CCT of 7272K. Commonly, the as-prepared blue-yellow phosphors are often lack of red component for the white light generation, that is cool white light, therefore, blue-orange and blue-red phosphors were investigated based on ET from $Eu^{2+}$ to $Mn^{2+}$ ions to obtain warm white light, such as $Ca_2PO_4Cl:Eu^{2+},Mn^{2+}$, $Na(Sr,Ba)PO_4:Eu^{2+},Mn^{2+}$, $Sr_{1.7}Mg_{0.3}SiO_{4-x}F_x:Eu^{2+},Mn^{2+}$, $Ca_9Lu(PO_4)_7:Eu^{2+},Mn^{2+}$, $Ca_{6-x-y}Mg_{x-z}(PO_4)_4:yEu^{2+},zMn^{2+}$, $Ba_2MgP_4O_{13}:Eu^{2+},Mn^{2+}$.[56] Good thermal stability for $Ca_2PO_4Cl:Eu^{2+},Mn^{2+}$ was observed in Fig. 4a. Moreover, the CIE color coordinates of (0.3102, 0.3096), a CCT of 4296 K, and CRI of 86 (Fig. 4b) when $Ca_2PO_4Cl:Eu^{2+}$, $Mn^{2+}$ was fabricated with a 400 nm n-UV chip. As a kind of cyan to pink phosphor $KCaY(PO_4)_2:Eu^{2+},Mn^{2+}$,[57] its tunable emission color can be generated based on the combination of emission bands, centered at 480 nm ($4f^65d^1 \rightarrow 4f^7$ transition of $Eu^{2+}$) and 652 nm ($^4T_1(^4G) \rightarrow {}^6A_1(^6S)$ transition of $Mn^{2+}$) in Fig 4c and d. When the emission bands of $Eu^{2+}$ in some hosts locate at green area, it can be possible to transfer it energy to $Mn^{2+}$ since the excitation bands of $Mn^{2+}$ locate at green region. Xia et al.[58] analyzed the $Eu^{2+}$ occupation site via the X-ray diffraction Rietveld analysis in detail, which indicated the preference of $Eu^{2+}$ occupying $Na^+$ sites in $NaScSi_2O_6$ host. An intense green emission can be observed with the emission peak at 533 nm upon 365 nm excitation. In $Eu^{2+},Mn^{2+}$ co-doped $NaScSi_2O_6$ phosphors, bright tunable color from green to yellow (Fig. 5a) with $Eu^{2+}$ emission band centered at 533 nm and $Mn^{2+}$ emission band centered at 654 nm can be observed under a 365 nm UV lamp excitation because of the ET from $Eu^{2+}$ to $Mn^{2+}$ ions through adjusting the concentration ratio of $Eu^{2+}$ and $Mn^{2+}$ ions. The ET mechanism from $Eu^{2+}$ to $Mn^{2+}$ was demonstrated to be a dipole-dipole (d-d) interaction by the analysis of equation (7). In addition, they combined the as-prepared phosphor $NaScSi_2O_6:0.05Eu^{2+},0.10Mn^{2+}$ and commercial blue BAM phosphors with 370 nm n-UV chip to produce the warm w-LED with the CIE color coordinate of (0.358, 0.378), CCT of 4666 K and good CRI of 92.2 (Fig. 5b). Similar green-yellow emission color took place in $Eu^{2+}$, $Mn^{2+}$ co-doped $Na_3LuSi_2O_7$ phosphors[59] with the corresponding $Eu^{2+}$ emission peak at 508 nm and $Mn^{2+}$ emission peak at 594 nm by adjusting the concentration ratio of $Eu^{2+}$ and $Mn^{2+}$ ions. Another four examples are $Eu^{2+}/Mn^{2+}$ co-doped

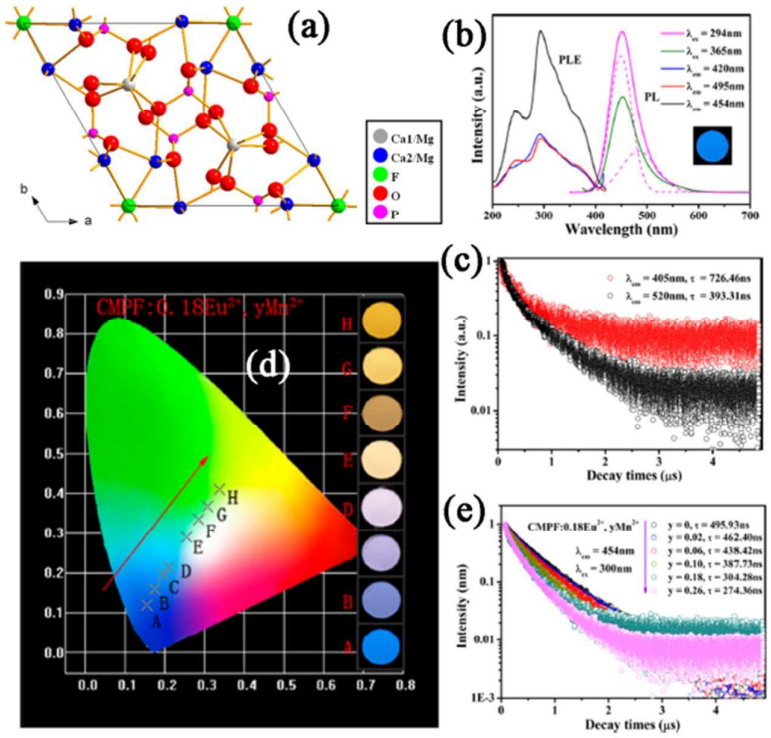


**Fig. 3** (a) Crystal structure of $Ca_9Mg(PO_4)_6F_2$ host. (b) Photoluminescence emission and excitation spectra of CMPF: $0.18Eu^{2+}$ sample with corresponding decay curves (monitored at 405 and 520 nm and excited at 300 nm), inset is the photograph excited under a 365 nm UV lamp. (c) CIE chromaticity coordination of CMPF:$0.18Eu^{2+}$,$yMn^{2+}$ samples (A–H corresponds to y = 0, 0.02, 0.06, 0.10, 0.18, 0.26, 0.34, 0.38, respectively.) with corresponding photographs excited under a 365 nm UV lamp on the right of the picture. (d) Decay curves and lifetimes of $Eu^{2+}$ in representative samples CMPF:$0.18Eu^{2+}$,$yMn^{2+}$ (monitored at 454 nm excited at 300 nm). (Reproduced with permission from ref. 51, copyright 2014, American Chemical Society.)

$Sr_3Y/Lu/Sc/Gd(PO_4)_3$.[60] In $Sr_3Lu(PO_4)_3:Eu^{2+},Mn^{2+}$, the CIE chromatic coordinate varied from green to yellow including white area (Fig. 5c) because their emission bands consisted of some appropriate blue, green and red components upon 355 nm excitation (Fig. 5d). The emission bands centered at 503 nm of $Eu^{2+}$ and 603 nm of $Mn^{2+}$ in $Ba_9Y_2Si_6O_{24}$ made them the tunable green-orange phosphors via the variation of doped ion concentration.[61] Huang et al. and Guo et al.[62,56d] investigated the photoluminescence properties of $(Ca/Sr/Mg)_9(Y/La/Gd/Lu)(PO_4)_7:Eu^{2+},Mn^{2+}$ phosphors, they found blue and red shifts occurred with increasing $Mg^{2+}$ and $Sr^{2+}$ concentrations, respectively, which is ascribed to the crystal field variation around $Eu^{2+}$ when $Ca^{2+}$ were substituted by smaller $Mg^{2+}$ and larger $Sr^{2+}$ in $Ca_9Y(PO_4)_7:Eu^{2+}$ (Fig. 6a). When the $Mn^{2+}$ ions was introduced into $Ca_{0.5}Sr_{0.5})_9Y(PO_4)_7:Eu^{2+}$, it showed tunable color from green to red by adjusting the $Eu^{2+}$ and $Mn^{2+}$ concentration ratio (Fig. 6b). They also combined the as-prepared $(Ca_{0.5}Mg_{0.5})_9Y(PO_4)_7$:0.007$Eu^{2+}$ and$(Ca_{0.5}Sr_{0.5})_9Y(PO_4)_7$:0.007$Eu^{2+}$, 0.02$Mn^{2+}$ with a 380 chip to generate w-LED with CCT of 6303 K, a CRI of 87.4, and CIE color coordinates x = 0.314 and y = 0.348 (Fig. 6c and d). The other two systems $Ca_9La/Gd(PO_4)_7:Eu^{2+},Mn^{2+}$ with similar properties were also considered to be the good candidate phosphors for n-UV pumped w-LED. Differently, the $Ca_9Lu(PO_4)_7:Eu^{2+},Mn^{2+}$ presented tunable cyan-pink including white emission color under 355 nm excitation because of a little different emission bands of $Eu^{2+}$ and $Mn^{2+}$ compared to similar samples above.

Generally, $Tb^{3+}$ is acted as an efficiently green-emitting activator based on its characteristic $^5D_4 \rightarrow {}^7F_{J(J=6,5,4,3)}$ transition.[63] Since the transition belongs to 4f-4f spin-forbidden transition, the absorption spectrum and emission band are rather weak and their widths are narrow. Therefore, it is desired to enhance its emission intensity via the ET effect. Herein, the sensitizer $Eu^{2+}$ is considered to be a good candidate to transfer its energy to $Tb^{3+}$.[64] In $Eu^{2+},Tb^{3+}$ co-doped phosphors, the emission color can be tuned from blue or cyan to green. Recently, Li et al. found that the tunable blue-green color can be produced via co-doping $Eu^{2+}$ and $Tb^{3+}$ into familiar β-$Ca_3(PO_4)_2$ compound with high quantum yields under UV excitation.[65] $Ba_3LaNa(PO_4)_3F:Eu^{2+},Tb^{3+}$ with apatite structure produced excellent ET properties from $Eu^{2+}$ to $Tb^{3+}$ ions, resulting in clear color variation from blue to green under a 365 UV lamp excitation (Fig. 7a) by adjusting the doped ions concentration ratio.[66] The ET mechanism from $Eu^{2+}$ to $Tb^{3+}$ ions was demonstrated to be electric dipole-quadrupole interaction using Inokuti-Hirayama (I-H) model showed in Introduction(Fig. 7b). Zhang et al.[67] developed a novel $Sr_3Y_2(Si_3O_9)_2:Eu^{2+},Tb^{3+}$ with corresponding structure reported. Tunable color from cyan to green can be observed from the emission spectra in Fig. 7c with increasing $Tb^{3+}$ concentration in $Sr_3Y_2(Si_3O_9)_2$:0.01$Eu^{2+}$,y$Tb^{3+}$ phosphors. Detailed schematic diagram of energy transfer (Fig. 7d) from $Eu^{2+}$ to $Tb^{3+}$ ion was used to understand the ET process. It showed some excited electrons in $Eu^{2+}$ $4f^65d^1$ energy level transfer their energy to $Tb^{3+}$ $^5D_4$ energy level, resulting in the $Tb^{3+}$ $^5D_4 \rightarrow {}^7F_{J(J=6,5,4,3)}$ transition.

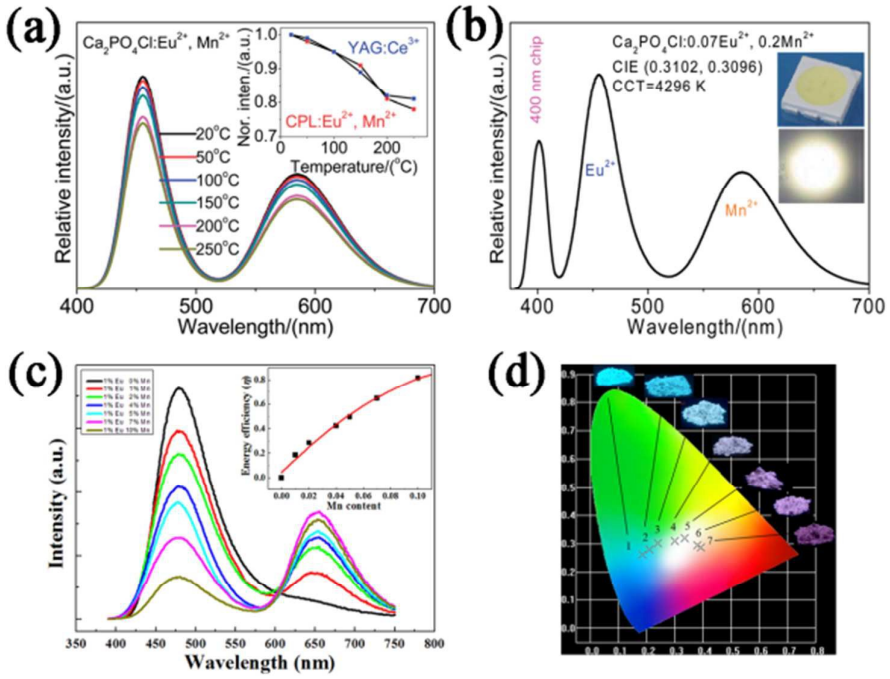


**Fig. 4** (a) Temperature-dependent emission spectra of $Ca_2PO_4Cl$:0.07$Eu^{2+}$,0.2$Mn^{2+}$ ($\lambda_{ex}$ = 370 nm). Inset: normalized intensity of $Ca_2PO_4Cl$:0.07$Eu^{2+}$,0.2$Mn^{2+}$ and YAG:Ce as a function of temperature. (b) Emission spectrum of a phosphor-converted LED (pc-LED) lamp fabricated with a 400 nm LED chip and warm, white-emitting phosphor $Ca_2PO_4Cl$:0.07$Eu^{2+}$,0.2$Mn^{2+}$. (c) PL spectra of a series of $KCaY(PO_4)_2$:1%$Eu^{2+}$,x%$Mn^{2+}$phosphors with different $Mn^{2+}$ concentrations (x = 0, 1, 2, 4, 5, 7, and 10 mol %) excited at 365 nm. (d) CIE coordinates of $KCaY(PO_4)_2$:1%$Eu^{2+}$,x%$Mn^{2+}$ phosphors (x = 0, 1, 2, 4, 5, 7, and 10). Insets show the phosphor images with different $Mn^{2+}$ doping concentrations excited at 365 nm in the ultraviolet (UV) box. (Reproduced with permission from ref. 56a and 57, copyright 2012, 2014, Royal Society of Chemistry, American Chemical Society.)

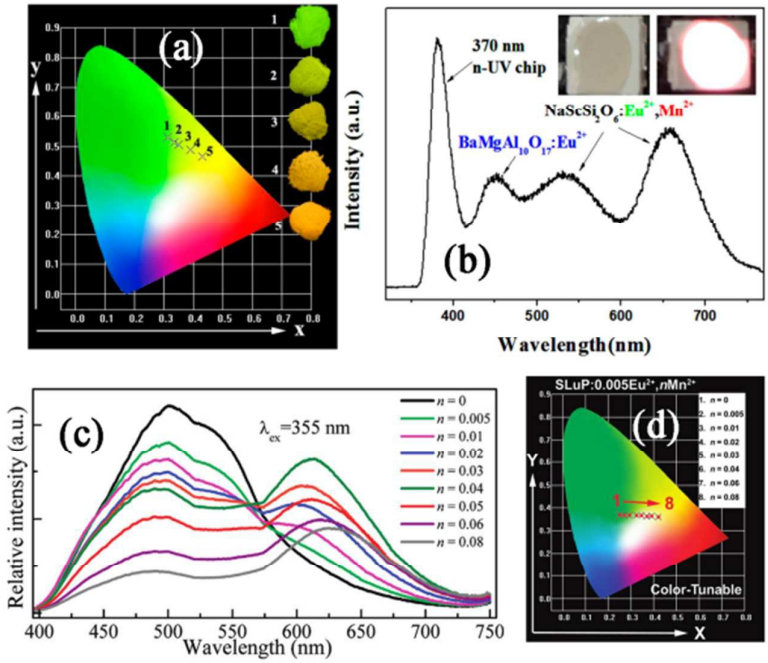


**Fig. 5** (a) CIE chromaticity diagram and a series of digital photographs of the selected $NaScSi_2O_6$:0.05$Eu^{2+}$,x$Mn^{2+}$ phosphors under 365 nm UV-lamp excitation. (b) Electroluminescence (EL) spectrum of the w-LED lamp based on the $NaScSi_2O_6$:0.05$Eu^{2+}$,0.10$Mn^{2+}$ and commercial blue BAM phosphors and driven by a current of 25 mA. The inset photographs are the w-LED lamp package. (c) PL spectra for $Sr_3Lu(PO_4)_3$:0.005$Eu^{2+}$,n$Mn^{2+}$ phosphors on $Mn^{2+}$ doping content (n) and (d) corresponding CIE chromaticity diagram for (point 1 to 8) excited at 355 nm. (Reproduced with permission from ref. 58 and 60b, copyright 2012, 2013, American Chemical Society.)

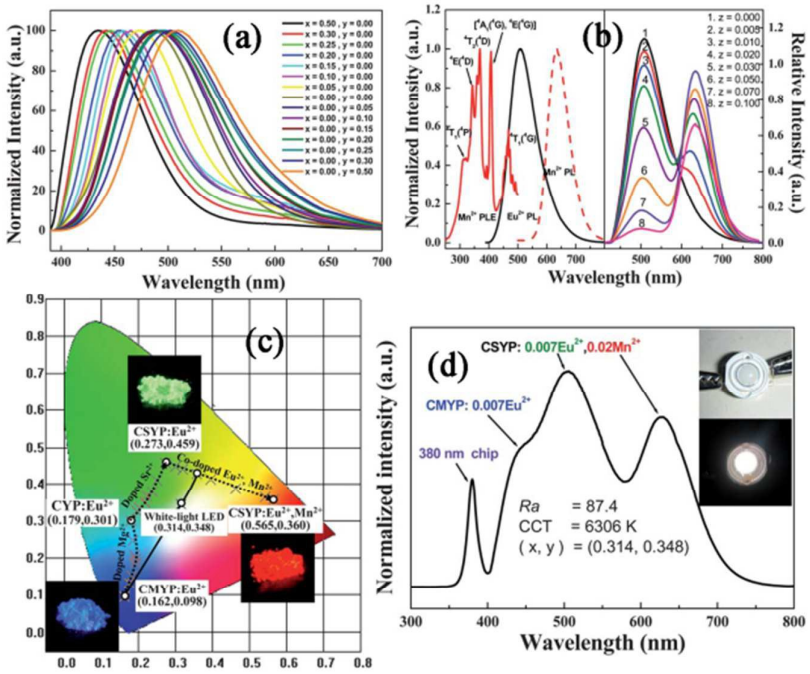


**Fig. 6** (a) Dependence of emission spectra of $(Ca_{0.993-x-y}Mg_xSr_y)_9Y(PO_4)_7$:0.007$Eu^{2+}$ phosphors on concentrations of $Mg^{2+}$ and $Sr^{2+}$. (b) Spectral overlap between $Eu^{2+}$ PL spectrum of $(Ca_{0.5}Sr_{0.5})_9Y(PO_4)_7$:$Eu^{2+}$ (black line) and PL excitation (PLE) spectrum of $(Ca_{0.5}Sr_{0.5})_9Y(PO_4)_7$:$Mn^{2+}$ (red line), and emission spectra of $Mn^{2+}$ at different values of z in $(Ca_{0.5}Sr_{0.5})_9Y(PO_4)_7$:0.007$Eu^{2+}$,z$Mn^{2+}$ phosphors excited at 380 nm. (c) CIE chromaticity diagram of $Ca_{9-x}Y(PO_4)_7$:0.007$Eu^{2+}$,x$Mg^{2+}$ (x = 0.05-0.5), $Ca_{9-y}Y(PO_4)_7$:0.007$Eu^{2+}$,y$Sr^{2+}$ (y = 0.05-0.5), and $(Ca_{0.5}Sr_{0.5-z})_9Y(PO_4)_7$:0.007$Eu^{2+}$,z$Mn^{2+}$ (z = 0-0.1) phosphors under 380 nm excitation. (d) EL spectrum of a white-emitting LED using a 380 nm n-UV chip comprising $(Ca_{0.5}Sr_{0.5})_9Y(PO_4)_7$:0.007$Eu^{2+}$,0.02$Mn^{2+}$ (yellow) and $(Ca_{0.5}Mg_{0.5})_9Y(PO_4)_7$:0.007$Eu^{2+}$ (blue) phosphors driven by a 350 mA current. (Reproduced with permission from ref. 62a, copyright 2011, Royal Society of Chemistry.)

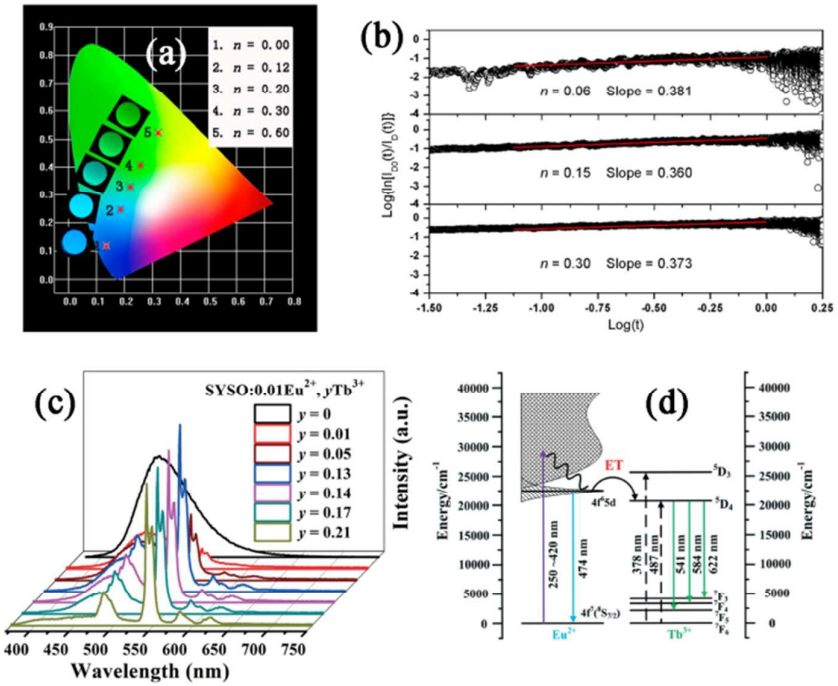


**Fig. 7** (a) CIE chromaticity diagram for $Ba_3LaNa(PO_4)_3F$:0.01$Eu^{2+}$,n$Tb^{3+}$ phosphors, together with their corresponding photographs under a 365 nm UV lamp. (b) Experimental data plots of log{ln[ID0(t)/ID(t)]} versus log(t) of $Eu^{2+}$ in $Ba_3LaNa(PO_4)_3F$:0.01$Eu^{2+}$,n$Tb^{3+}$ (n = 0.06, 0.15, 0.30) samples. The red lines indicate the fitting behaviors. (c) The PL spectra of $Sr_3Y_2(Si_3O_9)_2$:0.01$Eu^{2+}$,y$Tb^{3+}$ phosphors (y = 0, 0.01, 0.05, 0.13, 0.14, 0.17 and 0.21). (d) The schematic diagram of energy transfer in $Sr_3Y_2(Si_3O_9)_2$:$Eu^{2+}$,$Tb^{3+}$. (Reproduced with permission from ref. 66 and 67, copyright 2013, 2016, American Chemical Society, Royal Society of Chemistry.)

### 2.2 $Eu^{2+}$-$Tb^{3+}$-$Mn^{2+}$/$Eu^{3+}$/$Sm^{3+}$ systems

Since $Eu^{2+}$-$Tb^{3+}$ systems often produce tunable emission color from blue or cyan to green under UV/n-UV excitation, the supplement of red component in them is necessary if the white light is expected. As we know, the $Mn^{2+}$ can emit red color when it locates in the octahedron field, while $Eu^{3+}$ and $Sm^{3+}$ can emit their characteristic red emission based on their $^5D_0 \rightarrow {}^7F_2$ and $^4G_{5/2} \rightarrow {}^6H_{7/2}$ transitions, respectively. Therefore, co-doping $Mn^{2+}$,$Eu^{3+}$ or $Sm^{3+}$ in $Eu^{2+}$,$Tb^{3+}$ co-doped systems is possible to obtain white light emission.

In these three kinds of systems, the $Eu^{2+}$-$Tb^{3+}$-$Mn^{2+}$ system is the most frequent and efficient one. Lv et al.[68] designed and prepared the $BaMg_2Al_6Si_9O_{30}$:$Eu^{2+}$,$Tb^{3+}$,$Mn^{2+}$ phosphors, they found two emission peaks at 376 and 450 nm occurred in $Eu^{2+}$ singly- doped $BaMg_2Al_6Si_9O_{30}$ under 330 nm excitation since $Eu^{2+}$ occupied two kinds of $Ba^{2+}$ sites. $Mn^{2+}$ can emit the band around at 610 nm under 407 nm excitation because of its occupancy of $Mg^{2+}$ site with six-fold cordinated oxygens. Therefore, tunable color from blue to green and red inculding white were generated when $Tb^{3+}$ and $Mn^{2+}$ were codoped into it under UV excitation, respectively, based on the effective ET from $Eu^{2+}$ to $Tb^{3+}$ and $Mn^{2+}$ ions (Fig. 8a). In $Eu^{2+}$,$Mn^{2+}$ co-doped $KCaGd(PO_4)_2$ phosphors, the emission bands of $Eu^{2+}$ and $Mn^{2+}$ centered at 463 and 650 nm under 365 nm excitation. Liu et al.[69] added $Tb^{3+}$ into $Eu^{2+}$,$Mn^{2+}$ co-doped $KCaGd(PO_4)_2$ phosphors to compensate the green component, the green emission intensity increased with increasing $Tb^{3+}$ concentration (Fig. 8b), which made the emission color of $KCaGd(PO_4)_2$ $Eu^{2+}$,$Mn^{2+}$ shift from light red to white region under 365 nm excitation. A schematic level diagram for ET process in $Eu^{2+}$,$Tb^{3+}$,$Mn^{2+}$ co-doped $Ca_9Sc(PO_4)_7$ system[70] as a reference for $Eu^{2+}$,$Tb^{3+}$,$Mn^{2+}$ systems (Fig. 8c), we can see $Eu^{2+}$ emitted a band around 416 nm under 292 nm excitation, part of energy was transferred from $Eu^{2+}$ excited level to $^5D_3$ level of $Tb^{3+}$ and $^4A_1$ level of $Mn^{2+}$ to enhance their corresponding emission intensities. It is interesting some $Eu^{3+}$ were not been reduced in the reductive calcined atmosphere in Eu,$Tb^{3+}$ co-doped $LiBaBO_3$.[71] This phenomenon is not frequent. Xu et al. analyzed the ET properties from $Eu^{2+}$ to $Tb^{3+}$ and then to $Eu^{3+}$ via the variations of excitation spectra and fluorescent decay times in detail. The ET process of $Eu^{2+} \rightarrow (Tb^{3+})_n \rightarrow Eu^{3+}$ was relatively considerable, so they brought forward the branch model to explain the process of energy transfer for the terbium bridge in Fig. 8d. Firstly, when $Eu^{2+}$ ions were excited by UV light, it will give out a blue emission and sensitize $Tb^{3+}$ ions in the ground state. Then,the excited $Tb^{3+}$ ions may give out a green emission and transfer energy to $Eu^{3+}$, at the same time, the excited $Tb^{3+}$ ion may release energy in the way of cross-relaxation with another $Tb^{3+}$ ion in the ground state, and the $Tb^{3+}$ which absorbed the energy from excited $Tb^{3+}$ will also flow to $Eu^{3+}$ through the process of energy transfer. They utilized this property to obtain the color-tunable from blue-green to red emission under UV excitation. Jia et al.[72] had demonstrated $Tb^{3+}$ can act as an ET bridge to connect $Eu^{2+}$-$Sm^{3+}$ luminescent centers in $Sr_3Y(PO_4)_3$, realizing the red emission of $Sm^{3+}$ under near-UV excitation. However, it is a pity rare reports were connected to this condition.

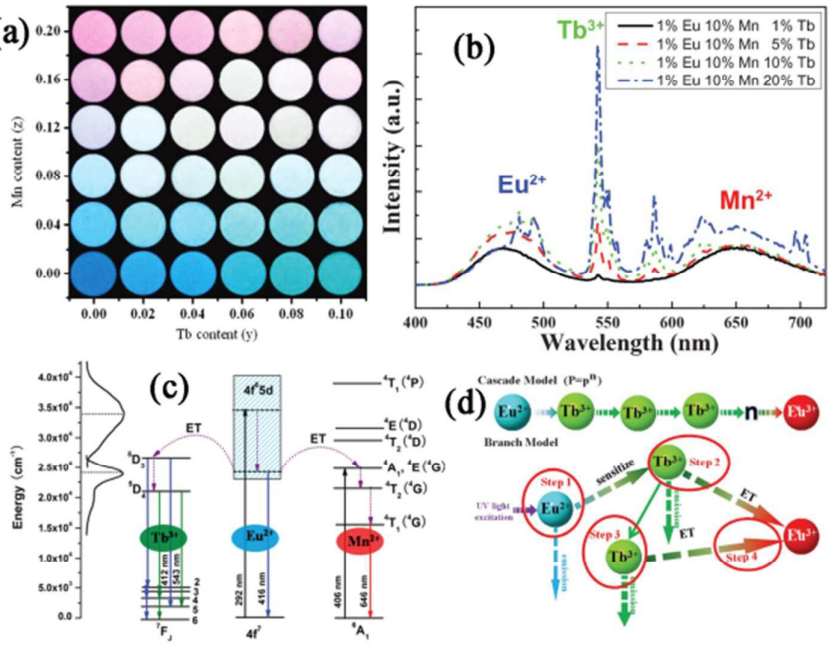


**Fig. 8** (a) The photographs of the emission $BaMg_2Al_6Si_9O_{30}$:0.04$Eu^{2+}$,y$Tb^{3+}$,z$Mn^{2+}$ phosphors with different percent of dopant contents (y and z) under excitation at 365 nm. (b) PL spectra of $KCaGd(PO_4)_2$:1%$Eu^{2+}$,10%$Mn^{2+}$ and y%$Tb^{3+}$ phosphors (y = 1, 5, 10, 20) excited at 365 nm. (c) The schematic level diagram for ET process from $Eu^{2+}$ to $Tb^{3+}$ and $Mn^{2+}$ in the $Ca_9Sc(PO_4)_7$ host. (d) ET models of the terbium chain (cascade model) and the terbium bridge (branch model). (Reproduced with permission from ref. 68-71, copyright 2011, 2013, 2015, American Chemical Society, Royal Society of Chemistry.)

### 2.3 $Ce^{3+}$-$Mn^{2+}$/$Tb^{3+}$/$Dy^{3+}$/$Eu^{2+}$ systems

It is well known $Ce^{3+}$ often produced n-UV to green emission under UV/n-UV excitation in many hosts.[73] Its high emission intensity and broad emission band are originated from its 4f-5d spin-allowed transition and phonon side band. Its emission spectra can overlap the excitation spectra of $Mn^{2+}$, $Tb^{3+}$, $Dy^{3+}$ or $Eu^{2+}$, which make it possible that ET from $Ce^{3+}$ to these ions take place when they are co-doped into proper hosts.[74] Therefore, tunable emission color can be generated in these systems.

As is presented in Section 2.1, emission color of $Mn^{2+}$ can vary from green to red depending on different coordinated fields. Therefore, tunable emission color from blue to green, yellow/orange, pink and red, and cyan or green to yellow/orange can be realized in $Ce^{3+}$-$Mn^{2+}$ system. Zhu et al. noticed that Tyutyunnik et al. reported a novel phase of $Sr_3Gd_2(Si_3O_9)_2$,[75] they tried to dope $Ce^{3+}$ and $Tb^{3+}$/$Mn^{2+}$ into it to investigate the PL properties of as-prepared samples and found that tunable color from blue to green and yellowish green including white were generated under UV excitation (Fig. 9a). Zhou et al.[76] prepared a kind of blue to yellow/orange color emission NaAlSiO4:$Ce^{3+}$,$Mn^{2+}$ phosphor based on two main emission bands centered at 430 and 590 nm and ET properties from $Ce^{3+}$ to $Mn^{2+}$ ions. The 430 nm emission band from $Ce^{3+}$ can be decomposed into four bands peaking at 404, 438, 470 and 519 nm, because $Ce^{3+}$ can occupy two kinds of $Na^+$ sites and its lowest 5d excited state to the $^2F_{5/2}$ and $^2F_{7/2}$ spin orbit 4f ground states. Fig. 9b presents the ET model for $Ce^{3+}$→$Mn^{2+}$ in the $NaAlSiO_4$ host as the reference in $Ce^{3+}$-$Mn^{2+}$ system. $Ce^{3+}$ absored the UV light from the ground state to the 5d excited state, and then efficiently transferred the energy to the $^4T_2$ level of $Mn^{2+}$. The excited free electron of $Mn^{2+}$ then relaxed to the excited state of $^4T_1$ ($^4G$) through $^4E$ ($^4D$), $^4T_2$ ($^4D$), ($^4E$, $^4A_1$) ($^4G$) and $^4T_2$ ($^4G$) intermediate energy levels by the process of nonradiation. Then the characteristic optical transition $^4T_1$→$^6A_1$ of $Mn^{2+}$ can be realized, which exhibited the characteristic emission of $Mn^{2+}$. Since red component is often deficient in phosphors, the red emission in $Ce^{3+}$,$Mn^{2+}$ systems also can be easily realized. Ci et al.[77] obtained a kind of $Ce^{3+}$, $Mn^{2+}$ co-doped phosphosilicate $Sr_7La_3[(PO_4)_{2.5}(SiO_4)_3(BO_4)_{0.5}](BO_2)$ phosphor with the apatite crystal structure ($P_{63/m}$), its emission color can be tuned from blue to pink with increasing $Mn^{2+}$ concentration(Fig. 9c). Moreover, they investigated the PL thermal quenching properties of $Ce^{3+}$ and $Mn^{2+}$ singly doped and $Ce^{3+}$,$Mn^{2+}$ co-doped samples. It was found the declines of emission intensities in singly $Ce^{3+}$ and $Mn^{2+}$ doped $Sr_7La_3[(PO_4)_{2.5}(SiO_4)_3(BO_4)_{0.5}](BO_2)$ were more less than that of $Ce^{3+}$ and $Mn^{2+}$ co-doped $Sr_7La_3[(PO_4)_{2.5}(SiO_4)_3(BO_4)_{0.5}](BO_2)$ at identical temperature. By comparing the different thermal quenching properties among them, they proposed a configurational coordinate diagram (Fig. 9d) which was very useful to understand the effect of temperature to PL in $Ce^{3+}$,$Mn^{2+}$ co-doped phosphors systems. It was suggested most of electrons return to the ground states along the red dotted line ① to bring out the orange emission of $Mn^{2+}$ and the blue dotted line ② to obtain the blue emission of $Ce^{3+}$ in respective $Mn^{2+}$ and $Ce^{3+}$ singly doped $Sr_7La_3[(PO_4)_{2.5}(SiO_4)_3(BO_4)_{0.5}](BO_2)$, ③ was added beside ① and ② processes, resulting in an enhancement of the $Mn^{2+}$ emission

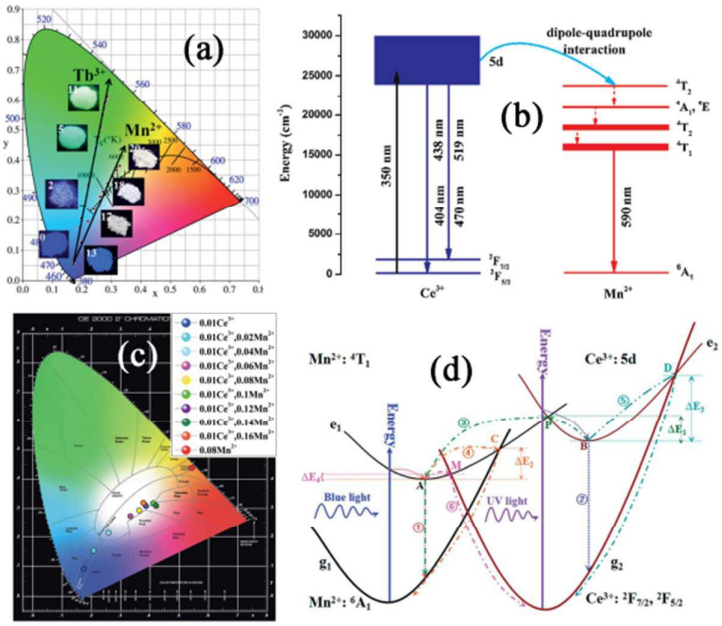


**Fig. 9** (a) The CIE chromaticity coordinates diagram for $Sr_3Gd_2(Si_3O_9)_2$:0.26$Ce^{3+}$,y$Tb^{3+}$ (y = 0, 0.02, 0.06, 0.10, 0.20, 0.40, 0.60, 0.80,1.00, 1.20, 1.40, 1.60, 1.74) and $Sr_3Gd_2(Si_3O_9)_2$:$Ce^{3+}$, z$Mn^{2+}$ (z = 0, 0.09, 0.21,0.33, 0.45, 0.57, 0.69, 0.81). (b) Illustration of the energy transfer model for $Ce^{3+}$→$Mn^{2+}$ in the $NaAlSiO_4$ host. (c) The Commission International CIE chromaticity coordinates of the samples $Sr_7La_3[(PO_4)_{2.5}(SiO_4)_3(BO_4)_{0.5}](BO_2)$:0.01$Ce^{3+}$, $Sr_7La_3[(PO_4)_{2.5}(SiO_4)_3(BO_4)_{0.5}](BO_2)$:0.08$Mn^{2+}$ and $Sr_7La_3[(PO_4)_{2.5}(SiO_4)_3(BO_4)_{0.5}](BO_2)$:0.01$Ce^{3+}$, x$Mn^{2+}$ (0.02⩽x⩽0.16). (d) Configurational coordinate diagram of the ground states of $Ce^{3+}$ and $Mn^{2+}$ and the excited states of $Ce^{3+}$ and $Mn^{2+}$. (Reproduced with permission from ref. 75-77, copyright 2014, 2015, 2016, Royal Society of Chemistry, Elsevier.)

intensity in $Ce^{3+}$,$Mn^{2+}$ co-doped sample. With increasing temperature, ④ and ⑤ were proceeded due to the stronger electron-phonon coupling in corresponding singly-doped samples. More electrons from e2 were transferred to e1 under the stronger phonon vibrations, which resulted in poorer thermal properties of $Ce^{3+}$ in $Sr_7La_3[(PO_4)_{2.5}(SiO_4)_3(BO_4)_{0.5}](BO_2)$:0.01$Ce^{3+}$,0.08$Mn^{2+}$ than those in $Sr_7La_3[(PO_4)_{2.5}(SiO_4)_3(BO_4)_{0.5}](BO_2)$:0.01$Ce^{3+}$. More electrons from e1 can return to the ground state along the pink dotted line ⑥, and this process also decreased the possibility of back tunneling of electrons from e1 to the e2, therefore leading to rapid degradation of the thermal properties of $Ce^{3+}$ and $Mn^{2+}$ in the $Sr_7La_3[(PO_4)_{2.5}(SiO_4)_3(BO_4)_{0.5}](BO_2)$:0.01$Ce^{3+}$,0.08$Mn^{2+}$ sample. Novel $Na_4Ca_4Si_6O_{18}$:$Ce^{3+}$,$Mn^{2+}$ and $NaCa_2LuSi_2O_7F_2$:$Ce^{3+}$,$Mn^{2+}$ phosphors[78] were also observed from blue to pink color under UV excitation. The ET mechanisms were analyzed to be both dipole-quadrupole interactions according to Dexter's ET expressions of multipolar interaction and Reisfeld's approximation[79], which were demonstrated via the consistence of calculations of $R_c$ by concentration quenching and spectral overlap methods. Zhang et al. and Sun et al.[80] reported $Ce^{3+}$,$Mn^{2+}$ co-doped $NaSrBO_3$ and $NaCaBO_3$ phosphors, the emission peaks located at 430 and 400 nm under 360 nm excitation in $NaSrBO_3$:$Ce^{3+}$ and $NaCaBO_3$:$Ce^{3+}$, respectively. Moreover, different $Mn^{2+}$ emission bands are centered at 630 and 600 nm, respectively. ET were deduced by the spectral overlap between $Ce^{3+}$ emission and $Mn^{2+}$ excitation bands and demonstrated via the declines of $Ce^{3+}$ fluorescent lifetimes with increasing $Mn^{2+}$ concentrations. Therefore, tunable emission color from blue to red were realized in these two systems.

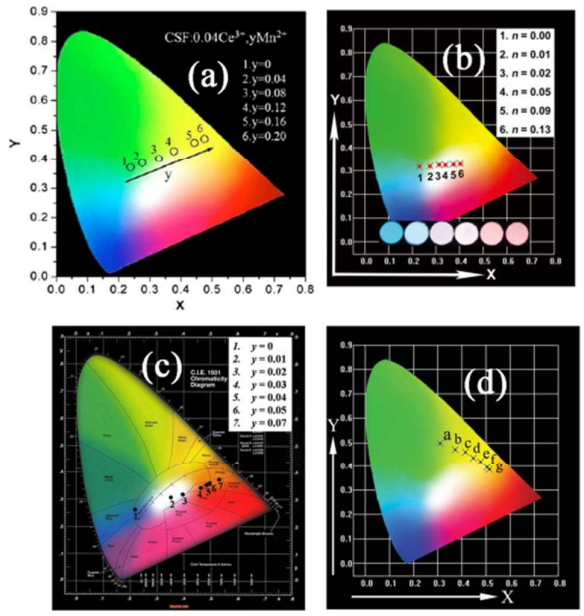


**Fig. 10** CIE chromaticity diagram of $Ca_4Si_2O_7F_2$:0.04$Ce^{3+}$,y$Mn^{2+}$ phosphors under 365 nm excitation (a), $Ca_2SrAl_2O_6$:0.01$Ce^{3+}$,0.01$Li^+$,n$Mn^{2+}$ with the excitation wavelength of 355 nm (b), $CaSr_2Al_2O_6$:0.03$Ce^{3+}$,0.03$Li^+$,y$Mn^{2+}$ under 358 nm excitation (c) and $Mg_{1.5}Lu_{1.5}Al_{3.5}Si_{1.5}O_{12}$:0.05$Ce^{3+}$,x$Mn^{2+}$ excited at 430 nm (d) (a-g, x = 0, 0.05, 0.10, 0.15, 0.20, 0.25, 0.35) phosphors with different doping concentrations of $Mn^{2+}$ ions. The inset in (b) shows the corresponding photographs of the samples under a 365 nm UV lamp. (Reproduced with permission from ref. 81-83 copyright 2011, 2012, 2014, Elsevier, Royal Society of Chemistry, American Chemical Society.)



 

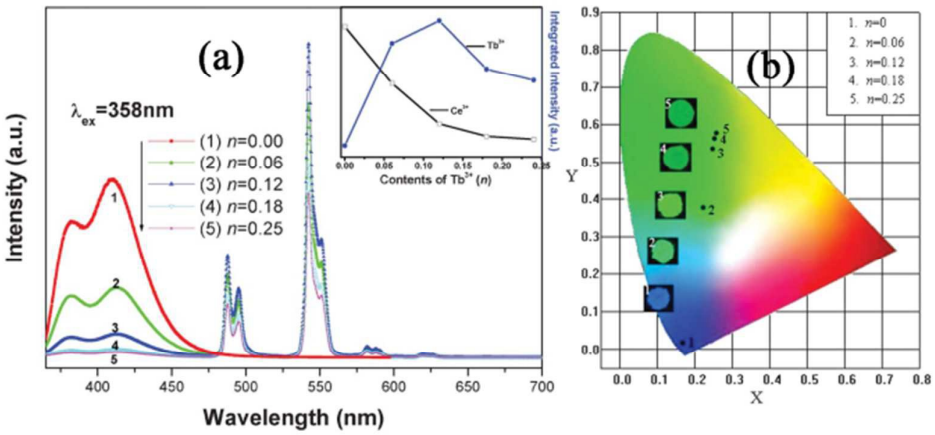


**Fig. 11** (a) PL spectra ($\lambda_{ex}$ = 358 nm) of $Na_2Gd_2B_2O_7$:0.05$Ce^{3+}$,n$Tb^{3+}$ (n = 0, 0.06, 0.12, 0.18, 0.25) with corresponding CIE diagram (b). Inset in (a) is the variation of integrated emission intensity of $Ce^{3+}$ and $Tb^{3+}$ with different concentration of $Tb^{3+}$. (Reproduced with permission from ref. 86e, copyright 2012, Royal Society of Chemistry.)

An asymmetric cyan-emitting band with many peaks including most intense one at about 455 nm was observed in $Ca_4Si_2O_7F_2$:$Ce^{3+}$ upon 330 nm excitation because there are four different $Ca^{2+}$ sites $Ce^{3+}$ located. Combined with $Mn^{2+}$ emission band centered at 580 nm, the $Ce^{3+}$,$Mn^{2+}$ co-doped $Ca_4Si_2O_7F_2$ samples can produce cyan to yellow color under 365 nm excitation (Fig. 11a) according to the CIE chromaticity diagram of $Ca_4Si_2O_7F_2$:0.04$Ce^{3+}$,y$Mn^{2+}$ with different y value.[81] Jiao et al. and Li et al.[82] prepared two novel $Ce^{3+}$,$Li^{+}$,$Mn^{2+}$ co-doped $Ca_2SrAl_2O_6$ and $CaSr_2Al_2O_6$ phosphors with identical crystal structure, in which $Li^{+}$ often acted as the charge compensator for $Ce^{3+}$. Therefore, similar PL properties were observed in them. Cyan color was observed because of broad emission bands of $Ce^{3+}$ with the range from 375 to 700 nm centered at 470 nm and from 375 to 625 nm centered at 460 nm, respectively with the excitations of 355 and 358 nm,respectively. After co-doping $Mn^{2+}$ into them, the emission color were tuned from cyan to light orange pink including white in phosphors with increasing $Mn^{2+}$ concentration (Fig. 11b and c). Differently, the ET mechanism from $Ce^{3+}$ to $Mn^{2+}$ ions is dipole-quadrupole interaction in $Ca_2SrAl_2O_6$:$Ce^{3+}$,$Mn^{2+}$ while quadrupole-quadrupole interaction in $CaSr_2Al_2O_6$:$Ce^{3+}$,$Mn^{2+}$ according to Dexter's and Reisfeld's theory. $Ce^{3+}$ and $Mn^{2+}$ co-doped $Mg_{1.5}Lu_{1.5}Al_{3.5}Si_{1.5}O_{12}$ with garnet crystal structure can emit green to yellow color under 430 nm excitation by varying concentrations of $Ce^{3+}$ and $Mn^{2+}$ (Fig. 11d).[83] It was attractive that tunable full-color-emitting $Ca_3Sc_2Si_3O_{12}$:$Ce^{3+}$,$Mn^{2+}$ phosphor was reported by Liu et al,[84] they analyzed that $Mn^{2+}$ would like to occupy not only $Ca^{2+}$ but also $Sc^{3+}$ sites because there was only one site for both $Ca^{2+}$ and $Sc^{3+}$, respectively, while two obvious emission peaks occurred in $Mn^{2+}$ singly-doped $Ca_3Sc_2Si_3O_{12}$. And the emission intensities of two $Mn^{2+}$ were enhanced and varied depending on $Mn^{2+}$ concentration, which is originated from different ET efficiencies from $Ce^{3+}$ to them in $Ca_3Sc_2Si_3O_{12}$:$Ce^{3+}$,$Mn^{2+}$, as well as compensation for the negative charge of $Mn^{2+}$ substitution for $Sc^{3+}$ in the form of $Ce^{3+}$ substitution for $Ca^{2+}$ by presence of $Ce^{3+}$ in $Ca_3Sc_2Si_3O_{12}$:$Ce^{3+}$,$Mn^{2+}$. Then, they added rare earth elements Y, La, Gd and Lu into $Ca_3Sc_2Si_3O_{12}$:$Ce^{3+}$,$Mn^{2+}$ phosphor[85] and investigated the effects of them to the PL properties in detail. It was found that the smaller the ionic radius, the larger the relative intensity of $Mn^{2+}$(II). The reason is that the smaller the ionic radius is, the easier the $Ln^{3+}$ at the $Ca^{2+}$ site to act as a charge compensator, resulting in the increasing $Mn^{2+}$ substitution at the $Sc^{3+}$ site. it is interesting the excitation band of as-prepared samples ranged from 200 to 500 nm centered at 450 nm, which is strongly matched with commercial blue InGaN chips. Therefore, By combinging this single $Ca_3Sc_2Si_3O_{12}$:$Ce^{3+}$,$Mn^{2+}$ phosphor with blue (450 nm) InGaN LED chips, pc-WLEDs with a high CRI of 91-92 and a CCT of 5379-6954 K were obtained.

In Section 2.1, we know that the green emission of $Tb^{3+}$ generally was utilized in phosphors based on its $^5D_4 \rightarrow {}^7F_{J(J=6,5,4,3)}$ transition. Similar with $Eu^{2+}$, $Ce^{3+}$ is also can be an effective sensitizer for $Tb^{3+}$ when $Ce^{3+}$ emission locates at ultraviolet to cyan area to overlap $Tb^{3+}$ excitation. Since the emission of $Tb^{3+}$ locates at green region, the emission color of $Ce^{3+}$,$Tb^{3+}$ co-doped samples would like to be tuned from ultraviolet/blue/cyan to green with different doping concentrations based on the ET from $Ce^{3+}$ to $Tb^{3+}$ ions under UV/n-UV excitation.

As is presented above, weak crystal field results in the short wavelength of $Ce^{3+}$ emission. Ultraviolet emissions occurred in many $Ce^{3+}$ hosts, which were overlapped with $Tb^{3+}$ characteristic excitation spectra. This deduced the ET from $Ce^{3+}$ to $Tb^{3+}$ ions. In phosphors $YBa_3B_9O_{18}$:$Ce^{3+}$,$Tb^{3+}$, $Sr_3Gd/La(PO_4)_3$:$Ce^{3+}$,$Tb^{3+}$, $KCaY(PO_4)_2$:$Ce^{3+}$,$Tb^{3+}$, $Na_2Gd_2B_2O_7$:$Ce^{3+}$,$Tb^{3+}$ and $NaCaPO_4$:$Ce^{3+}$,$Tb^{3+}$,[86] n-UV to green color can be observed with increasing $Tb^{3+}$ concentration with fixed $Ce^{3+}$ concentration. Taking $Na_2Gd_2B_2O_7$:$Ce^{3+}$,$Tb^{3+}$ as an example, we can see the variations of PL spectra ($\lambda_{ex}$ = 358 nm) of $Na_2Gd_2B_2O_7$:0.05$Ce^{3+}$,n$Tb^{3+}$ (n = 0, 0.06, 0.12, 0.18, 0.25) with different $Tb^{3+}$ concentration and the corresponding intensities in Fig. 11a. CIE diagram of these samples excited at 358 nm and digital PL photos under a 365 nm UV lamp excitation in Fig. 11b illustrated the color variation with $Tb^{3+}$ concentration change. It is well known that compounds with apatite structure had been demonstrated to be the good hosts for rare earth ions introductions. Recently, apatite $La_6(Sr/Ba)_4(SiO_4)_6F_2$:$Ce^{3+}$,$Tb^{3+}$, $Ca_4Y_6(SiO_4)_6O$:$Ce^{3+}$,$Tb^{3+}$, $MgGd_4Si_3O_{13}$:$Ce^{3+}$,$Tb^{3+}$, $Sr_2La_8(SiO_4)_6O_2$:$Ce^{3+}$,$Tb^{3+}$ besides β-

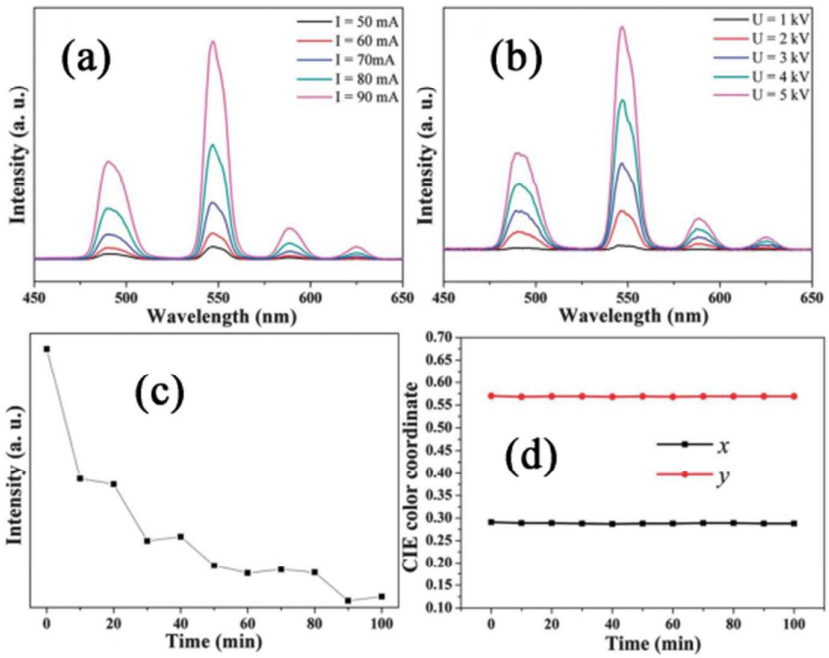


**Fig. 12** The CL spectra of $MgGd_4Si_3O_{13}$:0.08$Ce^{3+}$,0.7$Tb^{3+}$ with various (a) probe currents and (b) accelerating voltages. (c) The CL intensity and (d) the chromaticity coordinates depending on the electron beam bombardment time (min). (Reproduced with permission from ref. 87d copyright 2015, Royal Society of Chemistry.)

$Na_2Ca_4(PO_4)_2(SiO_4)$:$Ce^{3+}$,$Tb^{3+}$, $La_2Si_6O_3N_8$:$Ce^{3+}$,$Tb^{3+}$ and $Ba_3Y_2(BO_3)_4$:$Ce^{3+}$,$Tb^{3+}$ phosphors[87] were reported to show good ET properties from $Ce^{3+}$ to $Tb^{3+}$ ions to generate the tunable emission color from blue to green under UV excitation. Moreover, Zhou et al.[88d] investigated the cathodoluminescence (CL) properties of the $MgGd_4Si_3O_{13}$:$Ce^{3+}$,$Tb^{3+}$ samples. It appeared the CL intensity increased with the increase of filament current (Fig. 12a) and applied voltage (Fig. 12b) because larger filament current and applied voltage endowed the electrons with high energy, which penetrated more deeply into the phosphor body and stimulated a larger electron-beam current density and a higher CL intensity. The CL intensity was decreased by 15% when the bombing time reached 100 min (Fig. 12c). At the same time, the CIE values were nearly invariable under a continuous electron radiation for 1.5 h (Fig. 12d). The results supported the potential application of $MgGd_4Si_3O_{13}$:$Ce^{3+}$,$Tb^{3+}$ in FEDs. Xia et al.[88] reported the emission of $Ce^{3+}$ singly doped $Y_2Si_2O_7N_2$ was a broad asymmetric band, its peak shifted from 438 to 500 nm under 365 nm excitation with increasing $Ce^{3+}$ doped concentration from 0.005 to 0.20 (Fig. 13a). The phenomenon was explained by the ET between the optically active $Ce^{3+}$ ions in four $Y^{3+}$ crystallographic sites in Fig. 13b, leading to the concentration quenching. In addition, the red shift of the $Ce^{3+}$ emission correlated very well with the lattice expansion.[89] Therefore, the tunable emission from cyan to green can be observed with increasing $Tb^{3+}$ concentration y in $Y_4Si_2O_7N_2$:0.005$Ce^{3+}$,y$Tb^{3+}$ based on ET from $Ce^{3+}$ to $Tb^{3+}$, as depicted in Fig. 13c. The PL intensities decreased to 72.4% of the initial intensity for $Y_4Si_2O_7N_2$:$Ce^{3+}$,$Tb^{3+}$ phosphor under 365 nm excitation, corresponding to a temperature of 150 °C (Fig. 13d), which indicated its good thermal stability.

Systems with ET from $Ce^{3+}$ to $Dy^{3+}$ is much less than of $Ce^{3+}$-$Mn^{2+}$ or $Ce^{3+}$-$Tb^{3+}$ systems. Moreover, the ET effect is not obvious. Li et al.[90] prepared the $Ce^{3+}$,$Dy^{3+}$ co-doped borate $Sr_3Y_2(BO_3)_4$ phosphors. The emission spectrum of $Ce^{3+}$ had a wide band centered at 420 nm under 340 nm excitation in Fig. 14a(1), the excitation spectrum of $Dy^{3+}$ monitored at 576 nm consisted of many excitation lines between 250-500 nm exhibited in Fig. 14a(2). The spectral overlap of $Ce^{3+}$ emission and $Dy^{3+}$ excitation deduced possible ET from $Ce^{3+}$ to $Dy^{3+}$ ions. The similar excitation spectra monitored at 420 nm of $Ce^{3+}$ and 576 nm of $Dy^{3+}$ in Fig. 14a(3) was used to prove the ET from $Ce^{3+}$ to $Dy^{3+}$ ions. The ET modes from $Ce^{3+}$ to $Dy^{3+}$ in single-phase white-emitting $Ca_{20}A_{l26}Mg_3Si_3O_{68}$:$Ce^{3+}$,$Dy^{3+}$ was used to understand the ET process from $Ce^{3+}$ to $Dy^{3+}$ ions.[91] First, the electrons in $Ce^{3+}$ ground state absorbed the excited energy and jumped to 5d excited state, some of them produced the 5d-4f transition, some of them at lowest excited state transferred their energy to $Dy^{3+}$ $^4I_{13/2}$+$^4F_{7/2}$ energy levels, resulting in the $Dy^{3+}$ $^4F_{9/2}$→$^6H_{15/2}$ and $^4F_{9/2}$→$^6H_{13/2}$ after the non-radiate transition from $^4I_{13/2}$+$^4F_{7/2}$ to $^4F_{9/2}$ energy level. Geng et al.[92] synthesized the $Y_4Si_2N_2O_7$:$Ce^{3+}$,$Dy^{3+}$ phosphors via the soft-chemical ammonolysis method which is a good way to obtain nitride or oxynitride. Other $Ce^{3+}$-$Dy^{3+}$ ET systems such as $Zn_2P_2O_7$:$Ce^{3+}$,$Dy^{3+}$, $KNaCa(PO_4)_2$:$Ce^{3+}$,$Dy^{3+}$, GdOBr:$Ce^{3+}$,$Dy^{3+}$ and $Ca_6La_2Na_2(PO_4)_6F_2$:$Ce^{3+}$,$Dy^{3+}$ also can be referenced with the ET properties from $Ce^{3+}$ to $Dy^{3+}$ ions.[93]

It is common $Eu^{2+}$ can emit blue to red emission color originated from different crystal field strengths, as shown in Table 1. Sometimes, $Eu^{2+}$ also can be acted as an activator in $Ce^{3+}$,$Eu^{2+}$ co-doped systems while $Ce^{3+}$ acted as the sensitizer. Both of them are sensitive to the crystal field around. Therefore, the emission color can be realized from ultraviolet to blue and green, blue to green, yellow, and orange based on the ET from $Ce^{3+}$ to $Eu^{2+}$ ions in subsequently discussed systems.



 

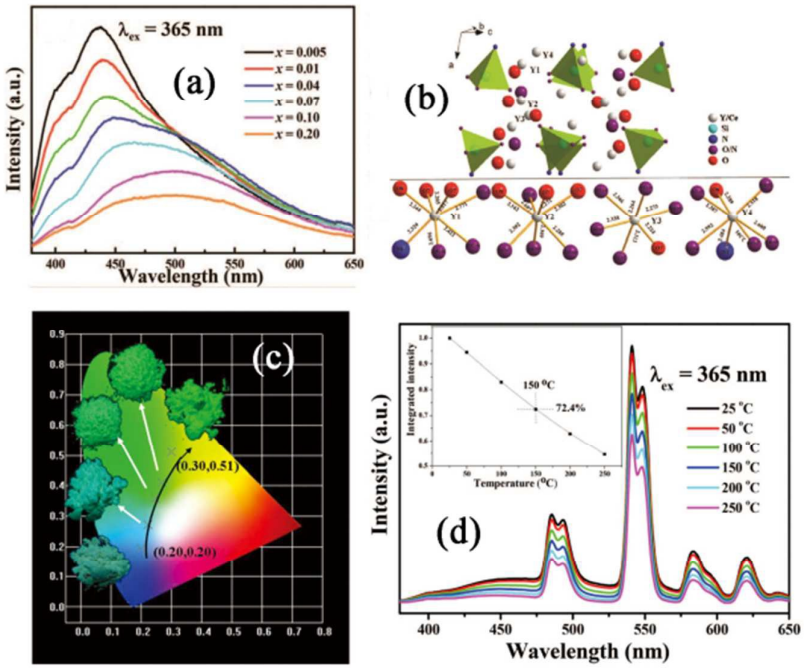


**Fig. 13** (a) PL ($\lambda_{ex}$ = 365 nm) spectra of $Y_4Si_2O_7N_2$:x$Ce^{3+}$ with varying $Ce^{3+}$ concentrations. (b) The crystal structure description of $Y_4Si_2O_7N_2$ showing the $Si(O,N)_4$ polyhedronand the coordination environment of the Y atoms with four different crystallographic sites. The related bond lengths are in the units of Å. (c) A representation of the CIE chromaticity coordinates for the $Y_4Si_2O_7N_2$:$Ce^{3+}$,$Tb^{3+}$ phosphors. (d) The temperature-dependent PL spectra of the $Y_4Si_2O_7N_2$:$Ce^{3+}$,$Tb^{3+}$ phosphor. (Reproduced with permission from ref. 88 copyright 2013, Royal Society of Chemistry.)

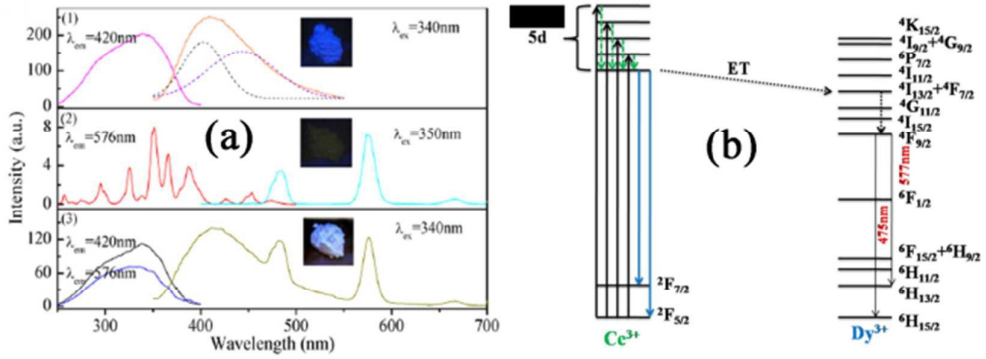


**Fig. 14** (a) PL and PLE spectra of (1) $Sr_3Y_2(BO_3)_4$:0.02$Ce^{3+}$, (2) $Sr_3Y_2(BO_3)_4$:0.10$Dy^{3+}$ and (3) $Sr_3Y_2(BO_3)_4$:0.02$Ce^{3+}$,0.10$Dy^{3+}$ samples; insets are luminescent photos of the corresponding samples under 365 nm xenon lamp excitation. (b) Decay curves of $Ce^{3+}$ in $Sr_3Y_2(BO_3)_4$:0.02$Ce^{3+}$,y$Dy^{3+}$ samples, inset shows lifetime and energy transfer efficiency versus $Dy^{3+}$ content. (c) Illustration of the energy transfer modes of $Ce^{3+}$→$Dy^{3+}$. (d) CIE chromaticity diagram for $Ca_{20}Al_{26}Mg_3Si_3O_{68}$:0.08$Ce^{3+}$,z$Dy^{3+}$(z = 0.01-0.09) phosphors excited at 345nm. (Reproduced with permission from ref. 90 and 91 copyright 2013, 2015, Elsevier.)

Zhou et al.[94] prepared the $Ce^{3+}$,$Eu^{2+}$ co-doped chloride phosphate $Sr_5(PO_4)_3Cl$ with apatite structure and investigated the PL and CL properties of as-prepared samples. They found the emission spectrum of $Ce^{3+}$ located at ultraviolet area, which was overlapped with the excitation spectrum of $Eu^{2+}$ in this host (Fig. 15a). Therefore, $Ce^{3+}$ may absorb the energy and transfer part of it to $Eu^{2+}$ to enhance the $Eu^{2+}$ emission. The emission intensity and fluorescent decay lifetimes of $Ce^{3+}$ monotonously decreased with increasing $Eu^{2+}$ concentration in $Sr_5(PO_4)_3Cl$:$Ce^{3+}$,$Eu^{2+}$ phosphors, which can be used to demonstrate the ET from $Ce^{3+}$ to $Eu^{2+}$ ions (Fig. 15b and c). This resulted in the tunable emission spectra from ultraviolet to blue upon 317 nm UV excitation. Moreover, they compared the CL emission spectra of $Sr_{4.98}Eu_{0.02}(PO_4)_3Cl$, $Sr_{4.96}Ce_{0.01}Eu_{0.02}Na_{0.01}(PO_4)_3Cl$, $Sr_{4.978}Ce_{0.001}Eu_{0.02}Na_{0.001}(PO_4)_3Cl$ and BAM (Fig. 15d). It can be seen that co-doped $Ce^{3+}$ and $Eu^{2+}$ $Sr_5(PO_4)_3Cl$ had the highest emission intensity, which illustrated the introduction of $Ce^{3+}$ in $Eu^{2+}$ doped $Sr_5(PO_4)_3Cl$:$Ce^{3+}$ is beneficial for the emission intensity. Tunable emission from ultraviolet to green in $Ba_3Si_6O_9N_4$:$Ce^{3+}$,$Eu^{2+}$,$K^+$ phosphors[95] can be inferred from the emission spectra of $Ba_{2.9-x}Eu_xCe_{0.01}K_{0.01}Si_6O_9N_4$ phosphors excited at 340 nm (from x = 0 to 0.01) (Fig. 15e). The energy level diagram

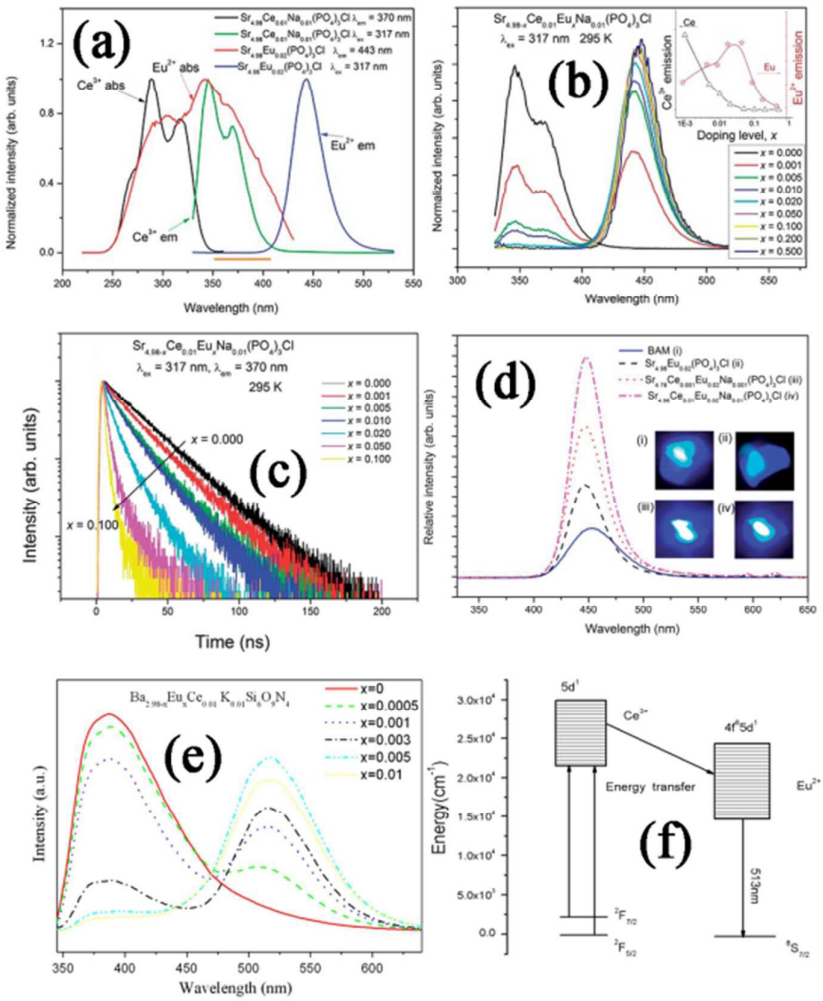


**Fig. 15** (a) Relative spectral locations of emission and excitation bands of $Ce^{3+}$ and $Eu^{2+}$ in $Sr_5(PO_4)_3Cl$ at 295 K. The maximum peak heights are normalized to 1.0. (abs absorption; em emission). (b) The emission spectra of $Sr_{4.98-x}Ce_{0.01}EuxNa_{0.01}(PO_4)_3Cl$ (x = 0.0-0.50) excited at 317 nm. The inset shows the relative emission intensity of $Ce^{3+}$ and $Eu^{2+}$ as a function of x. (c) Decay curves of $Ce^{3+}$ emission of $Sr_{4.98-x}Ce_{0.01}Eu_xNa_{0.01}(PO_4)_3Cl$ (x = 0.0-0.1) excited at 317 nm and monitored at 370 nm at 295 K. (d) CL spectra of $Sr_{4.98}Eu_{0.02}(PO_4)_3Cl$, $Sr_{4.96}Ce_{0.01}Eu_{0.02}Na_{0.01}(PO_4)_3Cl$, $Sr_{4.978}Ce_{0.001}Eu_{0.02}Na_{0.001}(PO_4)_3Cl$ and BAM (excitation voltage = 2 kV, current density = 100 mA $cm^{-2}$). (e) PL emission spectra of $Ba_{2.9-x}Eu_xCe_{0.01}K_{0.01}Si_6O_9N_4$ phosphors excited at 340 nm (from x = 0 to 0.01). (f) Schematic of the energy level system describing energy transfer in the $Ba_3Si_6O_9N_4:Ce^{3+},Eu^{2+},K^+$ phosphor. (Reproduced with permission from ref. 94 and 95 copyright 2013, 2014, Royal Society of Chemistry, Elsevier.)

involving energy transfer in the $Ba_3Si_6O_9N_4:Ce^{3+},Eu^{2+},K^+$ phosphor is shown in Fig. 15f. Electrons in two ground states of $^2F_{7/2}$ and $^2F_{5/2}$ with the energy gap of 2000 $cm^{-1}$ of $Ce^{3+}$ jumped to 5d energy level, then transferred part of energy to $Eu^{2+}$ 5d energy level and subsequently produced the $Eu^{2+}$ emission from 5d to ground $^8S_{7/2}$ level. When the emission band of $Ce^{3+}$ located at blue area, tunable emission color from blue to green occurred in $Ca_7Mg(SiO_4)_4:Ce^{3+},Eu^{2+}$, $Sr_2Al_2SiO_7:Ce^{3+},Eu^{2+}$, $CaSrAl_2SiO_7:Ce^{3+},Eu^{2+}$, and $Ba_4Si_6O_{16}:Ce^{3+},Eu^{2+}$ phosphors occurred based on the ET from $Ce^{3+}$ to $Eu^{2+}$ ion.[96] Fig. 16 shows the PL and corresponding CIE chromatic coordinates diagram of $Sr_2Al_2SiO_7:Ce^{3+},Eu^{2+}$. $Ce^{3+}$ emission band around 415 nm decreased and $Eu^{2+}$ emission band around 510 nm increased with increasing $Eu^{2+}$ concentration (Fig. 16a), which resulted in the CIE chromatic coordinates shift from blue to green area(Fig. 16b). Besides green, yellow and orange color also can be obtained in some $Ce^{3+}$-$Eu^{2+}$ co-doped phosphors.[97] A typical kind of phosphor $Sr_3Al_2O_5Cl_2:Ce^{3+},Eu^{2+}$ was investigated by Song et al.[97a] Fig. 17a shows the excitation and emission spectra of $Sr_3Al_2O_5Cl_2:0.01Ce^{3+},nEu^{2+}$ phosphors. The similar excitation spectra monitored at 444 nm ($Ce^{3+}$) and 609 nm ($Eu^{2+}$) along with the decline of intensity of $Ce^{3+}$ emission band and increase of $Eu^{2+}$ emission intensity with increasing $Eu^{2+}$ content illustrated the ET

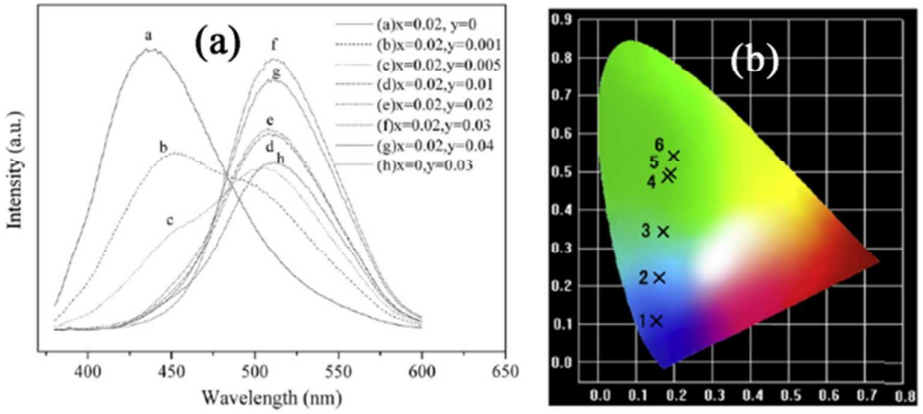


**Fig. 16** (a) PL emission spectra and corresponding CIE chromaticity diagram (b) for $Sr_{2-m-n}Al_2SiO_7$:$mCe^{3+}$,$nEu^{2+}$ phosphors excited at 345 nm. [(1-4 and 6) m = 0.02, n = 0, 0.001, 0.005, 0.02 and 0.03, (5) m = 0, n = 0.03]. (Reproduced with permission from ref. 96b copyright 2011, Elsevier.)

from $Ce^{3+}$ to $Eu^{2+}$, resulting in the tunable emission color from blue to yellow including white corresponding to the CIE chromatic coordinate diagram in Fig. 17b. The ET mechanism from $Ce^{3+}$ to $Eu^{2+}$ ions was analyzed to be dipole-dipole interaction on the basis of the theory of ET of Dexter. Moreover, a kind of blue-orange phosphors can be seen in $Ca_4(PO_4)_2O$:$Ce^{3+}$,$Eu^{2+}$ (Fig. 17c). $Ce^{3+}$ emitted a broad band centered at 460 nm under 380 nm excitation and $Eu^{2+}$ emitted a broad one around 650 nm under 460 nm excitation. Therefore, tunable emission from blue to orange via adjusting the doped ions concentrations corresponded to the CIE chromatic coordinate diagram in Fig. 17c. The w-LED lamp package emitted intense warm white light with a CCT of 4124 K, a color coordinate of (0.359, 0.310), and $R_a$ of 84 (Fig. 17d), which illustrated the potential as a single-composition white-emitting phosphor for w-LED applications.[97b]

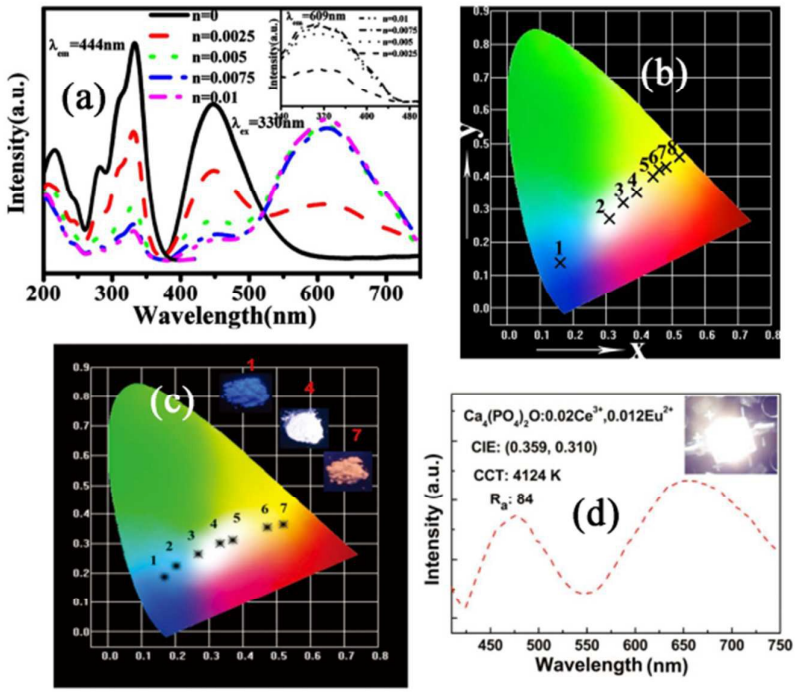


**Fig. 17** (a) Excitation and emission spectra of $Sr_3Al_2O_5Cl_2$:$0.01Ce^{3+}$,$nEu^{2+}$ phosphors. The inset is the excitation spectra monitored at 609 nm. (b) CIE chromaticity diagram for $Sr_3Al_2O_5Cl_2$:$mCe^{3+}$,$nEu^{2+}$ excited at 330 nm. (1-7, m = 0.01, n = 0, 0.0025, 0.003, 0.0035, 0.005, 0.0075, 0.01 and 8, m = 0, n = 0.04. and $Ca_4(PO_4)_2O$:$0.02Ce^{3+}$,$yEu^{2+}$ phosphors (y = 0, 0.002, 0.006, 0.010, 0.012, 0.022, and 0.026) (c). Insets in (c) show the phosphor images with different $Eu^{2+}$ doping concentrations excited at 380 nm. (d) Electroluminescence spectrum of $Ca_4(PO_4)_2O$:$0.02Ce^{3+}$,$0.012Eu^{2+}$ phosphor-based w-LED under a current of 700 mA. The inset shows a photograph of the LED package. (Reproduced with permission from ref. 97 copyright 2009, 2015, AIP Publishing, Royal Society of Chemistry.)

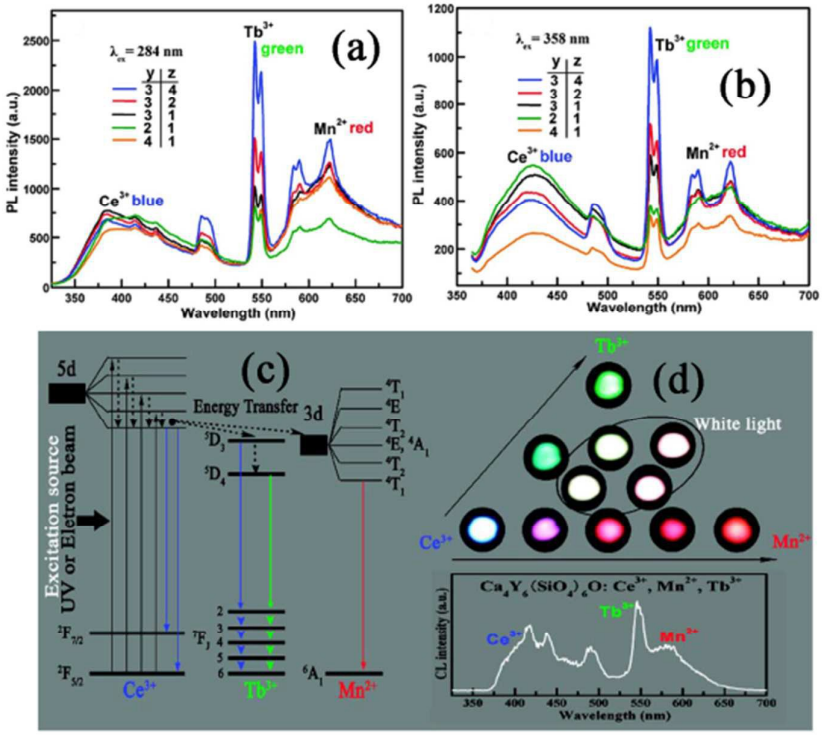


**Fig. 18** PL spectra of $Ca_4Y_6(SiO_4)_6O$:10mol% $Ce^{3+}$,ymol% $Mn^{2+}$,z mol% $Tb^{3+}$ samples (y = 2, 3, 4; z = 1, 2, 4) under different wavelengths UV excitation: (a) 284 nm and (b) 358 nm. (c) Illustration of the energy transfer modes of $Ce^{3+}$→$Tb^{3+}$/$Mn^{2+}$ and luminescent photographs of $Ca_4Y_6(SiO_4)_6O$:10mol% $Ce^{3+}$,ymol% $Mn^{2+}$,zmol% $Tb^{3+}$ samples: y = 0, 1, 3, 5, 8, z = 0, y = 0, z = 2, 8, y = 3, z = 1, 2, y = 4, 5, z = 2. The CL emission spectrum belongs to the representative sample of $Ca_4Y_6(SiO_4)_6O$:10mol% $Ce^{3+}$,3 mol% $Mn^{2+}$,2mol% $Tb^{3+}$. (Reproduced with permission from ref. 98b copyright 2012, American Chemical Society.)

### 2.4 $Ce^{3+}$-$Tb^{3+}$-$Mn^{2+}$/$Eu^{3+}$/$Sm^{3+}$ systems

Similar with $Eu^{2+}$-$Tb^{3+}$-$Mn^{2+}$/$Eu^{3+}$/$Sm^{3+}$ systems, the $Ce^{3+}$-$Tb^{3+}$-$Mn^{2+}$/$Sm^{3+}$/$Eu^{3+}$ systems were also can be the candidates to obtain white emission because $Mn^{2+}$/$Sm^{3+}$/$Eu^{3+}$ can supply the red component in $Ce^{3+}$,$Tb^{3+}$ systems. Therefore, many researchers have devoted their interest to them. Li et al. and Liu et al.[98] investigated the PL and CL properties of $Ce^{3+}$,$Tb^{3+}$,$Mn^{2+}$ co-doped three kinds of oxyapatite $Mg_2Y_8(SiO_4)_6O_2$, $Ca_4Y_6(SiO_4)_6O$ and$Sr_{3.5}Y_{6.5}O_2(PO_4)_{1.5}(SiO_4)_{4.5}$. Taking $Ca_4Y_6(SiO_4)_6O$:$Ce^{3+}$,$Tb^{3+}$,$Mn^{2+}$ as the example, we can see the emission spectra consisted of $Ce^{3+}$, $Tb^{3+}$ and $Mn^{2+}$ bands centered at blue, green and red regions under 284 and 358 nm (Fig. 18a and b), therefore, it can generate white emission with appropriately doping contents of $Ce^{3+}$, $Tb^{3+}$ and $Mn^{2+}$. In this condition, the ET process from $Ce^{3+}$ to both $Tb^{3+}$ and $Mn^{2+}$ ions were displayed with the corresponding energy level diagram in Fig. 18c. Electrons in $Ce^{3+}$ 4f ground state absorbed excited energy to jump to 5d excited state, then they nonradiatively relaxed to lowest 5d excited state of it, some of them produced the 5d-4f transition, and some transferred their energy to $Tb^{3+}$ $^5D_3$ and $Mn^{2+}$ 3d energy levels, resulting in the $^5D_3$→$^7F_{J\ (J=6,5,4,3,2)}$ and $^5D_4$→$^7F_{J\ (J=6,5,4,3)}$ transitions of $Tb^{3+}$ and $^4T_1$→$^6A_1$ transition of $Mn^{2+}$. CL emission color in Fig. 18d displayed blue to green and red in $Ca_4Y_6(SiO_4)_6O$:$Ce^{3+}$,$Tb^{3+}$ and $Ca_4Y_6(SiO_4)_6O$:$Ce^{3+}$,$Mn^{2+}$ phosphors, respectively. And white light was produced after co-doping $Ce^{3+}$,$Tb^{3+}$,$Mn^{2+}$ into $Ca_4Y_6(SiO_4)_6O$, best CIE chromatic coordinate can reach (0.328, 0.331) for $Ca_4Y_6(SiO_4)_6O$:10mol% $Ce^{3+}$,3mol% $Mn^{2+}$,2mol% $Tb^{3+}$ sample. The CL intensity of this sample increased with increasing filament current and accelerating voltage, which is attributed to the deeper penetration of the electrons into the phosphor body and the larger electronic beam current density. The electron penetration depth can be expressed using empirical equation:[99]

$$L\left(\overset{\circ}{A}\right) = 250\left(\frac{A}{\rho}\right)\left(\frac{E}{\sqrt{Z}}\right)^n \qquad (13)$$

where *A* represents the atomic or molecular weight of the material, *ρ* represents the bulk density, *Z* is the atomic number or the number of electrons per molecule in the compounds, and *E* corresponds to the accelerating voltage (kV).[100] Therefore, the deeper the electron penetration depth, the more plasma would be produced, resulting in more activator ions being excited, and thus the CL intensity increased. Moreover, our group also synthesized the $Ca_9Bi(PO_{4)7}$:$Ce^{3+}$,$Tb^{3+}$,$Mn^{2+}$ and $Ca_5(PO_4)_2SiO_4$:$Ce^{3+}$/$Tb^{3+}$/$Mn^{2+}$ phosphors.[101] Results showed white light can be generated under UV excitation or low-voltage electron beam excitation. Good thermal quenching properties of these two kinds of samples indicated them to be as the candidate phosphors for LEDs and FEDs. Other systems[102] such as $NaCaBO_3$: $Ce^{3+}$,$Tb^{3+}$,$Mn^{2+}$, $Ca_3Al_2O_6$:$Ce^{3+}$,$Tb^{3+}$,$Mn^{2+}$, $Ca_9MgNa(PO_4)_7$:$Ce^{3+}$/$Tb^{3+}$/$Mn^{2+}$ and $BaMg_2(PO_4)_2$:$Ce^{3+}$,$Mn^{2+}$,$Tb^{3+}$ combined the $Ce^{3+}$ blue emission, $Tb^{3+}$ green emission and $Mn^{2+}$ red emission to acquire white light based on the ET from $Ce^{3+}$ to $Tb^{3+}$ and $Mn^{2+}$ in a single host.

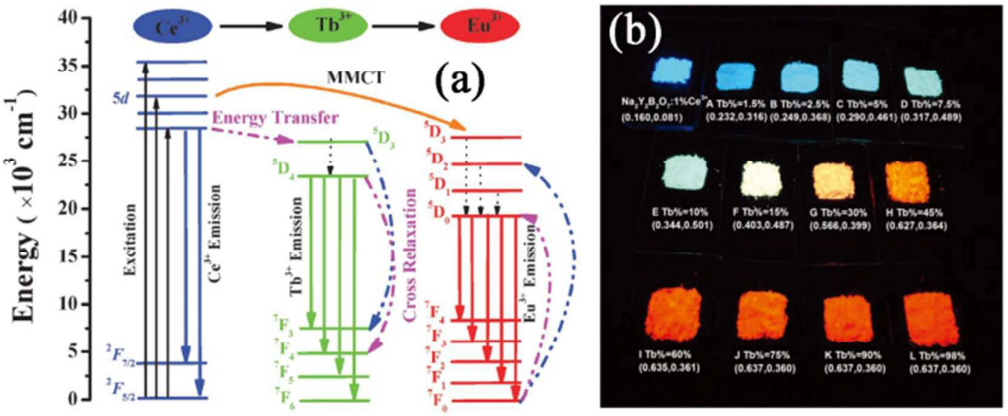


**Fig. 19** (a) Energy level model for the energy processes of $Ce^{3+}$→$Tb^{3+}$→$Eu^{3+}$ in $Na_2Y_2B_2O_7$ host. (b) Pictures of the samples of $Na_2Y_2B_2O_7$:1% $Ce^{3+}$ and $Na_2Y_2B_2O_7$:1% $Ce^{3+}$,z$Tb^{3+}$,1% $Eu^{3+}$ (A–L) under a 365 nm UV box with the corresponding chromaticity coordinates. (Reproduced with permission from ref. 104 copyright 2013, Royal Society of Chemistry.)

In some systems, $Eu^{3+}$ may not be reduced to $Eu^{2+}$ in reductive atmosphere in some host. However, the energy transfer from $Ce^{3+}$ to $Eu^{3+}$ is not considered to be effectively proceeded because of metal-metal charge transfer physical process of $Ce^{3+}$+$Eu^{3+}$→$Ce^{4+}$+$Eu^{2+}$.[103] However, $Tb^{3+}$ can transfer its energy to $Eu^{3+}$ in many hosts (which will be discussed below), therefore it can be acted as the bridge to form the terbium chain between $Ce^{3+}$ and $Eu^{3+}$ ions and result in the effective ET from $Ce^{3+}$ to $Eu^{3+}$ ions, which is expressed as $Ce^{3+}$→$Tb^{3+}$⋯$Tb^{3+}$→$Eu^{3+}$ process. The emission color tuned from blue to yellow or orange based on the combination of $Ce^{3+}$ blue emission, $Tb^{3+}$ green emission and $Eu^{3+}$ red emission. Wen et al.[104] successfully designed the terbium chain in the form of $Ce^{3+}$ →$(Tb^{3+})_n$→$Eu^{3+}$ in the $Na_2Y_2B_2O_7$ host by the ET processes from $Ce^{3+}$ to $Tb^{3+}$ and $Tb^{3+}$ to $Eu^{3+}$ ions. The ET properties of $Ce^{3+}$ to $Tb^{3+}$ and $Tb^{3+}$ to $Eu^{3+}$ were demonstrated by the declines of decay lifetimes of $Ce^{3+}$ and $Tb^{3+}$ together with the variations of emission spectra in $Ce^{3+}$,$Tb^{3+}$ and $Tb^{3+}$,$Eu^{3+}$ co-doped $Na_2Y_2B_2O_7$, respectively. The ET details were depicted in Fig. 19a. Firstly, $Ce^{3+}$ ions can be effectively excited by n-UV light and jumped from the ground state ($^2F_{5/2}$) to the excited states (5d energy levels). Then, $Ce^{3+}$ ions decayed to the lowest vibrational level of the excited state and gave out the excess energy to their surroundings, subsequently returned to the state of $^2F_{7/2}$ or $^2F_{5/2}$ simultaneously by a radiative process or ET to $^5D_3$ level of $Tb^{3+}$ ions. The probability for ET of $Ce^{3+}$→$Tb^{3+}$ increased with increasing concentration of $Tb^{3+}$ attributed to more neighbouring $Tb^{3+}$ ions around $Ce^{3+}$ ions. Cross relaxation $^5D_3$ + $^7F_6$ = $^5D_4$ + $^7F_0$ resulted in the characteristic emission of $^5D_4$→$^7F_J$ (J = 6,5,4,3) transition.[105] As the content of $Tb^{3+}$ increased, the distances of $Tb^{3+}$-$Tb^{3+}$ and $Tb^{3+}$-$Eu^{3+}$ shortened, leading to the quenching of $Tb^{3+}$ emission and the enhancement of the ET from $Tb^{3+}$ to $Eu^{3+}$, which may be ascribed to the following mechanism:[106]

$$Tb^{3+}\left(^5D_4\right)+Eu^{3+}\left(^7F_0\right)+\Delta E_{ph}\rightarrow Tb^{3+}\left(^7F_4\right)+Eu^{3+}\left(^5D_0\right) \quad (14)$$

$$Tb^{3+}\left(^5D_3\right)+Eu^{3+}\left(^7F_0\right)\rightarrow Tb^{3+}\left(^7F_3\right)+Eu^{3+}\left(^5D_2\right)+\Delta E_{ph} \quad (15)$$

where $\Delta E_{ph}$ is the phonon energy and relatively low ($\leqslant$500 $cm^{-1}$). Ultimately, the energy level of $^5D_2$ relaxes to $^5D_0$ and emission of $Eu^{3+}$ ions will be given out because of the characteristic transition of $^5D_0$→$^7F_J$ (J = 1,2,3,4) and the possibility of metal-metal charge transfer effect dropped. After optimization, the emission colors of as-prepared samples tuned from blue to orange by only adjusting the $Tb^{3+}$ concentration in $Na_2Y_2B_2O_7$:1% $Ce^{3+}$,z$Tb^{3+}$,1% $Eu^{3+}$ (A-L) in Fig. 19b. Using the ET properties from $Ce^{3+}$ to $Tb^{3+}$ and then to $Eu^{3+}$, many researcher obtained the abundant emission colors including white light under UV/n-UV excitation in many recent systems such as $BaY_2Si_3O_{10}$:$Ce^{3+}$,$Tb^{3+}$,$Eu^{3+}$, $(Y/Gd)_2SiO_5$:$Ce^{3+}$,$Tb^{3+}$,$Eu^{3+}$, $GdBO_3$:$Ce^{3+}$,$Tb^{3+}$,$Eu^{3+}$.[107]

Although the system of $Eu^{2+}$-$Tb^{3+}$-$Sm^{3+}$ is rarely utilized to obtain abundant emission colors, the $Ce^{3+}$-$Tb^{3+}$-$Sm^{3+}$ system has been successfully designed to obtain tunable emission color based on the ET from $Ce^{3+}$ to $Tb^{3+}$ and then to $Sm^{3+}$. Fig. 20a shows the PL emission spectra of as-prepared $La_5Si_2BO_{13}$:0.01$Ce^{3+}$,y$Tb^{3+}$,0.01$Eu^{3+}$/$Sm^{3+}$ (y = 0.10, 0.30, 0.50) phosphors under 300 nm excitation,[108] which were used to verify the bridge of $Tb^{3+}$ to sensitize $Eu^{3+}$/$Sm^{3+}$, herein the $Eu^{3+}$/$Sm^{3+}$ content was fixed as 0.01 to alleviate the metal-metal charge transfer effect. It is found that low $Tb^{3+}$ concentration is hard to form a terbium bridge to transfer $Ce^{3+}$ energy to $Eu^{3+}$/$Sm^{3+}$ because the metal-metal charge transfer process was not suppressed. However, strong narrow band of $Eu^{3+}$/$Sm^{3+}$ red emission is exhibited when y = 0.30 and 0.50, which illustrated that a terbium bridge was successfully formed and efficient $Ce^{3+}$-$Tb^{3+}$-$Eu^{3+}$/$Sm^{3+}$ ET was realized. The red emission intensity increased with increasing $Tb^{3+}$ content to 0.50 since the empirical saturation distance ($R_c$) is 6–7 Å for $Tb^{3+}$ bridge when $Tb^{3+}$ concentration was 0.50.Therefore, tunable color from blue to red was realized in this system under UV excitation. Yu et al.[109] exploited this effect to add the $Tb^{3+}$ into $CaYAl_3O_7$:$Ce^{3+}$,$Sm^{3+}$ to enhance the sensitization effect, they proposed the schematic energy-level diagram to explain the luminescence process and the possible energy-transfer pathways in $CaYAl_3O_7$:$Ce^{3+}$,$Tb^{3+}$,$Sm^{3+}$ in Fig. 20b. The $Ce^{3+}$ to $Tb^{3+}$ energy transfer process was depicted in $Ce^{3+}$-$Tb^{3+}$-$Eu^{3+}$ system above, which is not described here. In the $Tb^{3+}$→$Sm^{3+}$ scheme, electrons in excited state $^5D_4$ level of $Tb^{3+}$ can transferred their energy to $^4G_{9/2}$ level of $Sm^{3+}$ first. Then the $Sm^{3+}$ ions at $^4G_{9/2}$ level relaxed non-radiatively to $^4G_{7/2}$

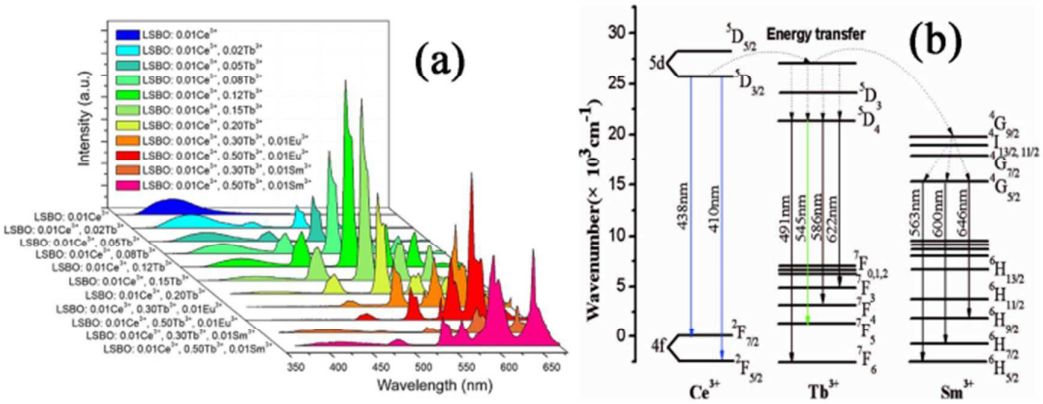


**Fig. 20** (a) The PL spectra ($\lambda_{ex}$ = 280 nm) of $La_5Si_2BO_{13}$:$Ce^{3+}$,$Tb^{3+}$,$Eu^{3+}$/$Sm^{3+}$ samples under 300 nm UV excitation. (b) Schematic energy-level diagram explaining the luminescence process and the possible energy-transfer pathways for the $CaYAl_3O_7$:0.05$Ce^{3+}$,y$Tb^{3+}$, 0.04$Sm^{3+}$. (Reproduced with permission from ref. 108 and 109 copyright 2014, 2015, The Electrochemistry Society, Elsevier.)

and $^4G_{5/2}$ and subsequently decayed radiatively to the ground state $^4H_{5/2}$, $^4H_{7/2}$ and $^4H_{9/2}$ corresponding to the emissions peaking at 563, 600 and 646 nm, respectively. Therefore, the emission color was tuned from blue to white based on the ET process of $Ce^{3+}$→$Tb^{3+}$→$Sm^{3+}$.

### 2.5 $Bi^{3+}$/$Tb^{3+}$-$Eu^{3+}$/$Sm^{3+}$ systems

As displayed in Table 1, $Bi^{3+}$ can emit different colors from blue to orange under UV excitation originated from its $^3P_1$→$^1S_0$ transition. Utilizing $Bi^{3+}$ as the sensitizer with blue emission to transfer its energy to $Eu^{3+}$/$Sm^{3+}$ is an alternative method to enhance $Eu^{3+}$/$Sm^{3+}$ red emission intensity and obtain tunable emission color from blue to red.

Frequently, $Bi^{3+}$ was used to enhance the red emission of $Eu^{3+}$. The addition of $Bi^{3+}$ in $CaMoO_4$:$Eu^{3+}$, $Sr_{0.5}Ca_{0.5}MoO_4$:$Eu^{3+}$, $CaWO_4$:$Eu^{3+}$ and $Ca_3Ti_2O_7$:$Eu^{3+}$ phosphors[110] can enhance the red emission of $Eu^{3+}$ under characteristic line excitation of $Eu^{3+}$ with different extents. However, the reasons for the enhancements were not identical. In $CaMoO_4$:$Eu^{3+}$, authors speculated the $Bi^{3+}$-induced red emission enhancement may result from the increase of the $^7F_0$ →$^5L_6$ and $^7F_0$→$^5D_2$ absorption strengths since the lifetime of $^5D_0$ reduced slightly with increasing $Bi^{3+}$ concentration x in $CaMoO_4$:x$Bi^{3+}$,0.05$Eu^{3+}$, indicating that the quantum efficiency of $^5D_0$→$^7F_2$ emission was hardly affected by $Bi^{3+}$. More odd-rank crystal field components were induced by crystal structural distortion and the decrease of symmetry with the addition of $Bi^{3+}$, leading to more opposite parity components, for example, $4f^5$5d states, mixed into the $4f^6$ transitional levels of $Eu^{3+}$. While in $Sr_{0.5}Ca_{0.5}MoO_4$:$Eu^{3+}$, the enhancement of $Eu^{3+}$ emission was attributed to the ET between $Bi^{3+}$ and $Eu^{3+}$ together with the change in the symmetry of $Eu^{3+}$ after the addition of $Bi^{3+}$. In $CaWO_4$:$Eu^{3+}$, several reasons were proposed including the distortion of $Eu^{3+}$ ion symmetry and the red shift of charge transfer, moreover, they reckoned that the electro-dipole transition can borrow intensity from the lowest strong absorption band to improve the emission intensity of $^5D_0$→$^7F_2$ transition. In $Ca_3Ti_2O_7$:$Eu^{3+}$, the enhancement of $Eu^{3+}$ red emission was mainly ascribed to the ET from $Bi^{3+}$ to $Eu^{3+}$ ions. It can be found that the emission band centered at 411 nm became dominant and the 490 nm emission band gone weak in $BaY_2Si_3O_{10}$:$Bi^{3+}$ phosphors with increasing excitation wavelength,[48,111] as depicted in Fig. 21a, which illustrated $Bi^{3+}$ ions were experiencing different local environments, namely $Bi^{3+}$(I) and $Bi^{3+}$(II). In other words, $Bi^{3+}$ ions substituted two different crystallographic sites in the host lattice, resulting in the different emission bands. Spectral overlap between $Bi^{3+}$ emission and $Eu^{3+}$ excitation (Fig. 21b) together with variation of emission spectra (Fig. 21c) were used to prove the ET from $Bi^{3+}$ to $Eu^{3+}$ ions. Schematic energy level diagram in Fig. 21d clearly describes the ET process from $Bi^{3+}$ to $Eu^{3+}$ ions. Electrons in $Bi^{3+}$ ground state $^1S_0$ jumped to its $^3P_1$ excited state after absorption of excitation energy, and some of them transfer their energy to $Eu^{3+}$ $^5L_6$ energy level, resulting in the $^5D_2$→$^7F_0$ and $^5D_0$→$^7F_{J\ (J=1,2,3,4,5)}$ transition emission of $Eu^{3+}$ after the non-radiate transition of $^5L_6$ to $^5D_2$ and $^5D_0$. Utilizing the $Bi^{3+}$(I) and $Bi^{3+}$(II) and $Eu^{3+}$ emissions, the white light can be obtained under appropriate excitation (Fig. 21e). In $Sr_2Y_8(SiO_4)_6O_2$:$Bi^{3+}$/$Eu^{3+}$, $Y_2O_3$:$Bi^{3+}$,$Eu^{3+}$, $Gd_2O_3$:$Bi^{3+}$,$Eu^{3+}$, $MgY_2Si_3O_{10}$:$Bi^{3+}$,$Eu^{3+}$, $Sr_3Lu_2(BO_3)_4$:$Bi^{3+}$,$Eu^{3+}$ systems,[112,10f,] similar properties were observed, which inspires us that $Bi^{3+}$-$Eu^{3+}$ system may also be an alternative way to acquire white light emission under UV excitation. Recently, our group found a novel kind of $Bi^{3+}$,$Eu^{3+}$ co-doped $Ba_3Y_4O_9$ phosphor.[113] The emission color can be tuned from yellowish green to orange red under a 365 nm UV lamp excitation, as depicted in Fig. 21f, which rarely took place in $Bi^{3+}$,$Eu^{3+}$ co-doped phosphors. The ET properties from $Bi^{3+}$ to $Sm^{3+}$ had ever been observed in $Bi^{3+}$,$Sm^{3+}$ co-doped $Ca_3Al_2O_6$ system, but the ET effect was relatively worse than that of $Bi^{3+}$-$Eu^{3+}$ system.[114]

As depicted above, the $Tb^{3+}$ can act as the bridge to transfer $Eu^{2+}$ or $Ce^{3+}$ energy to $Eu^{3+}$ or $Sm^{3+}$ ions to enhance the red emission. Therefore, herein we reviewed some $Tb^{3+}$-$Eu^{3+}$/$Sm^{3+}$ systems to illustrate the efficient ET from $Tb^{3+}$ to $Eu^{3+}$ or $Sm^{3+}$ without $Eu^{2+}$ or $Ce^{3+}$. The emission color will be tuned from cyan/green to orange/red under characteristic excitation of $Tb^{3+}$. Zeng et al.[115] investigated the $Tb^{3+}$ and $Eu^{3+}$ co-doped fluorapatite $Ba_3GdK(PO_4)_3F$. They chose the $Tb^{3+}$ concentration 0.05 as the sensitizer content with several stronger emission lines of $^5D_3$→$^7F_{J\ (J=6,5,4,3,2)}$ transition compared with $^5D_4$→$^7F_{J\ (J\ =\ 6,5,4,3)}$ transition. Therefore, both emission intensities of $^5D_3$ and $^5D_4$ transitions decreased with the

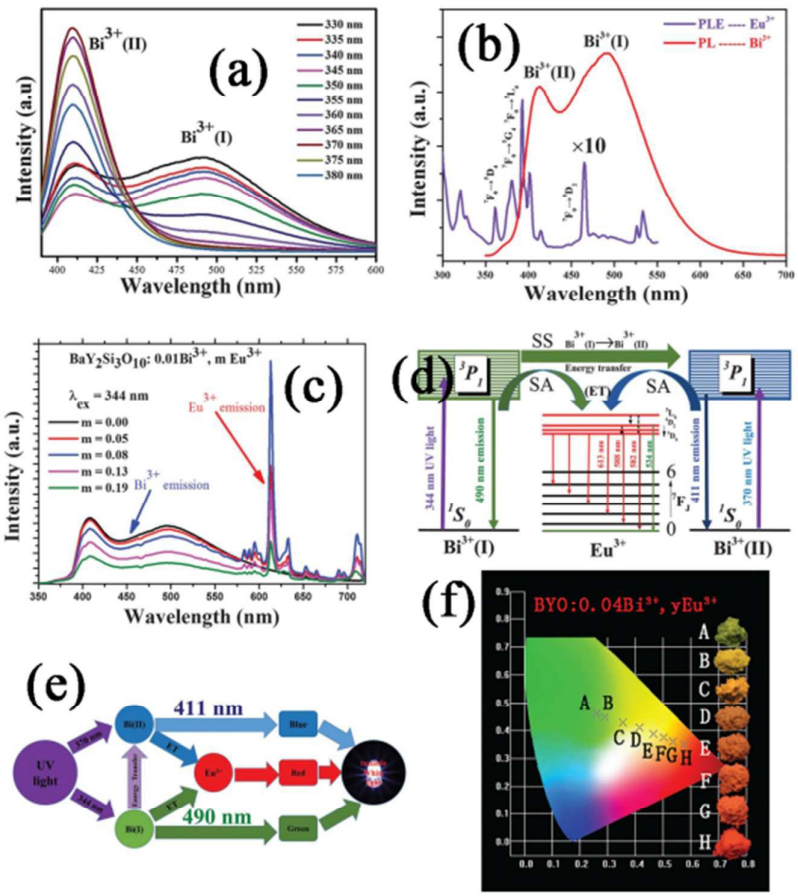


**Fig. 21** (a) The PL spectra of $BaY_2Si_3O_{10}$:0.01$Bi^{3+}$ pumped by different excitation wavelengths $\lambda_{ex}$ = 330–380 nm. (b) The spectral overlap between the PL spectrum ($\lambda_{ex}$ = 344 nm) of $BaY_2Si_3O_{10}$:0.01$Bi^{3+}$ and the PLE spectrum ($\lambda_{em}$ = 613 nm) of $BaY_2Si_3O_{10}$:0.13$Eu^{3+}$. (c) PL ($\lambda_{ex}$ = 344 nm) spectra of $BaY_2Si_3O_{10}$:0.01$Bi^{3+}$,m$Eu^{3+}$ (m = 0.00, 0.05, 0.08, 0.13 and 0.19) with different $Eu^{3+}$ dopant concentrations. (d) Schematic energy level diagram of energy transfer SS:$Bi^{3+}$(I)→$Bi^{3+}$(II) and SA:$Bi^{3+}$(I)/$Bi^{3+}$(II)→$Eu^{3+}$. (e) The scheme of generating emission-tunable white light emission and energy transfer routes upon UV light excitation. (f) Variation of the CIE chromatic coordinates as a function of $Eu^{3+}$ concentration y in $Ba_3Y_4O_9$:0.04$Bi^{3+}$,y$Eu^{3+}$ (A-H, y = 0, 0.04, 0.08, 0.12, 0.16, 0.20, 0.24, 0.32) samples under 346 nm excitation (Inset are digital photographs of the luminescent samples under a 365 nm UV lamp excitation). (Reproduced with permission from ref. 111 and 113 copyright 2015, Royal Society of Chemistry.)

increase of $Eu^{3+}$ concentration n in $Ba_3GdK(PO_4)_3F$:0.05$Tb^{3+}$,n$Eu^{3+}$ under 276 nm excitation (Fig. 22a), contrary to that of $Eu^{3+}$, which was originated from the ET from $Tb^{3+}$ to $Eu^{3+}$ ions. The ET mechanism was demonstrated to be dipole-dipole interactions according to Dexter's ET formula. Schematic energy level diagram depicted the ET from $Tb^{3+}$ to $Eu^{3+}$ in $Ba_3GdK(PO_4)_3F$:0.05$Tb^{3+}$,n$Eu^{3+}$ in Fig. 22b. First, electrons were excited to the $^5D_4$ or $^5D_3$ state of $Tb^{3+}$ after multistep relaxations. Then, some of them shifted from the $^5D_4$ or $^5D_3$ excited state to the $^7F_J$ ground state, resulting in generation of green or cyan light. Meanwhile, some may transfer their energy to the $^5D_1$ excited state of $Eu^{3+}$ ions. Finally, red light would be given out due to the electrons relax to $^5D_0$ state and $^5D_0$→$^7F_{J\ (J\ =\ 1,\ 2,\ 3,\ 4)}$ transitions of $Eu^{3+}$ ions. Based on the ET from $Tb^{3+}$ to $Eu^{3+}$, Zhou et al. and Zhang et al. designed the $Tb^{3+}$,$Eu^{3+}$ co-doped $La_3GaGe_5O_{16}$ and $KCaY(PO_4)_2$ to obtain the tunable emission color from green to orange and orange red under 377 and 365 nm UV lamp excitation, respectively.[116]

Besides $Tb^{3+}$-$Eu^{3+}$ system, $Tb^{3+}$ also can effectively transfer its energy to $Sm^{3+}$ under characteristic excitation of $Tb^{3+}$ to gain tunable emission color from green to orange or red. However, the different emission colors were taken place under different excitation wavelengths. Xie et al.[117] depicted the ET process via the energy level diagram in $CaLa_2(MoO_4)_4$:$Tb^{3+}$,$Sm^{3+}$ phosphor in Fig. 23. Under 277 nm excitation, electrons in ground state $^7F_6$ were excited to $^5D_{2,3,4}$ state of $Tb^{3+}$, then they nonradiatively relaxed to the $^5D_4$ energy level, some of them produced transition of $^5D_4$→$^7F_{J\ (J\ =\ 6,5,4,3)}$, and some transferred energy to $^4G_{7/2}$ of $Sm^{3+}$, then relaxed to $^4G_{5/2}$ and generated $^4G_{5/2}$→$^6H_{J\ (J\ =\ 5/2,7/2,9/2)}$ transitions, resulting in the red emission of $Sm^{3+}$. This can be as a reference of ET process from $Tb^{3+}$ to $Sm^{3+}$ ions in co-doped samples. The ET mechanism was certified to be dipole-dipole interactions according to Dexter's ET formula. The ET phenomenon from $Tb^{3+}$ to $Sm^{3+}$ ions in some other systems such as $Ba_3LaNa(PO_4)_3F$:$Tb^{3+}$,$Sm^{3+}$, $K_3Gd(PO_4)_2$:$Tb^{3+}$,$Sm^{3+}$, $Ca_2La_8(GeO_4)_6O_2$:$Tb^{3+}$,$Sm^{3+}$ also can be observed with tunable emission color.[118]

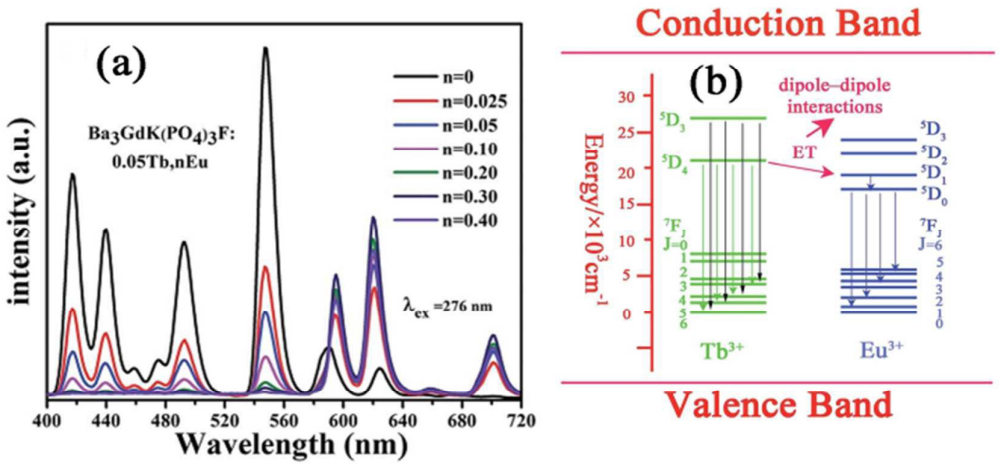


**Fig. 22** (a) PL spectra of $Ba_3GdK(PO_4)_3F$:0.05$Tb^{3+}$,n$Eu^{3+}$ phosphors excited at 276 nm. (b) Schematic energy level diagram displaying the energy transfer among $Tb^{3+}$ and $Eu^{3+}$ in $Ba_3GdK(PO_4)_3F$:$Tb^{3+}$,$Eu^{3+}$ phosphor. (Reproduced with permission from ref. 115, copyright 2015, Royal Society of Chemistry.)

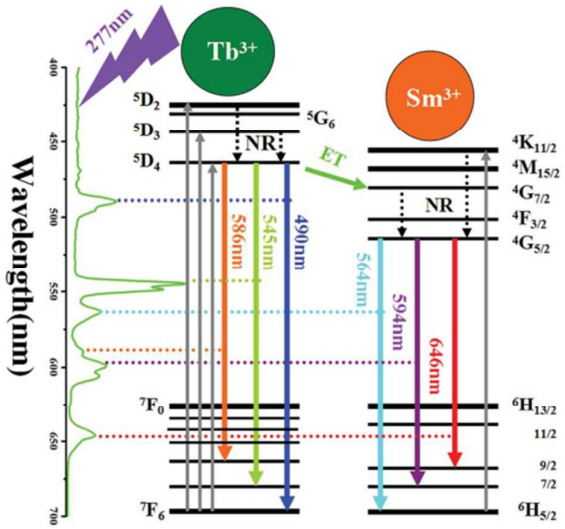


**Fig. 23** Schematic energy-level diagram showing the excitation and emission mechanisms of $CaLa_2(MoO_4)_4$:$Tb^{3+}$,$Sm^{3+}$ phosphors (ET: energy transfer; NR: nonradiative relax). (Reproduced with permission from ref. 117, copyright 2015, Royal Society of Chemistry.)

## 3. Conclusions

In this review article, we summarized the recently development of phosphors potentially applied in LEDs and FEDs with different emission colors under UV/n-UV excitation based on the ET effect between sensitizers and acceptors. The sensitizers can be $Eu^{2+}$, $Ce^{3+}$, $Bi^{3+}$ and $Tb^{3+}$, and the activators were $Mn^{2+}$, $Eu^{2+}$, $Tb^{3+}$, $Dy^{3+}$, $Sm^{3+}$ and $Eu^{3+}$. Many systems involving $Eu^{2+}$-$Mn^{2+}$/$Tb^{3+}$, $Eu^{2+}$-$Tb^{3+}$-$Mn^{2+}$/$Eu^{3+}$/$Sm^{3+}$, $Ce^{3+}$-$Mn^{2+}$/$Tb^{3+}$/$Dy^{3+}$/$Eu^{2+}$, $Ce^{3+}$-$Tb^{3+}$-$Mn^{2+}$/$Eu^{3+}$/$Sm^{3+}$, $Bi^{3+}$-$Eu^{3+}$/$Sm^{3+}$ and $Tb^{3+}$-$Eu^{3+}$/$Sm^{3+}$ were presented in the paper. Moreover, the emission color can be tuned from blue to green, yellow, orange and even pink/red, cyan to green, yellow, orange and pink/red, green to yellow and orange and so on including white. Since there are two main kinds of current alternative ways containing the combinations of UV/n-UVLED chips with blue, green, and red phosphors, or single-phase full-color phosphors to obtain w-LEDs, the phosphors is one of important components in them, moreover, it is also an indispensable part for FEDs. Therefore, the investigations of phosphors with different emission colors based on ET still need to be continued. However, it is still a great challenge that the phosphors with appropriate excitation and emission spectra, high energy conversion efficiency, excellent thermal quenching property are expected to be discovered. Simultaneously, the fabricated w-LEDs with appropriate phosphors need produce high CRI (>80) and low CCT (<4500 K). The phosphors with blue, green, red emissions are better to be narrow bands to alleviate the reabsorption of blue by green and red components when they are mixed to fabricate w-LEDs, besides, they should have the close attenuating speeds to reduce the variations of CIE chromatic coordinates. As for single-phase full-color phosphors,

the efficiency is the primary issue to be solved urgently. In FEDs, the phosphors should have good conductivity so that they have intense emission under low-voltage electron-beam excitation. Although many phosphors systems have been investigated by researchers, the theory calculation and simulation of PL properties for doping ions in different crystal structures is rarely investigated. Therefore, combing it with experimental data is an alternative to guide the further design of phosphors in the future.

## Acknowledgements

This project is financially supported by the National Natural Science Foundation of China (NSFC Grants 51472234, 51172227, 21521092, 91433110), National Basic Research Program of China (Grants 2014CB643803), and Joint Funds of the National Natural Science Foundation of China (Grant U1301242).

## References

1 (a) S.-S. Wang, W.-T. Chen, Y. Li, J. Wang, H.-S. Sheu and R.-S. Liu, *J. Am. Chem. Soc*., 2013, **135**, 12504; (b) R.-J. Xie, N. Hirosaki, M. Mitomo, Y. Yamamoto, T. Suehiro and K. Sakuma, *J. Phys. Chem. B*, 2004, **108**, 12027; (c) Y. Liu, D. Tu, H. Zhu and X. Chen, *Chem. Soc. Rev*., 2013, **42**, 6924; (d) H. A. Hoppe, *Angew. Chem. Int. Ed*., 2009, **48**, 3572; (e) Q. Dai, M. E. Foley, C. J. Breshike, A. Lita and G. F. Strouse, *J. Am. Chem. Soc*. 2011, **133**, 1547.

2 (a) J. H. Oh, S. J. Yang and Y. R. Do, *Light*: *Sci. Appl*., 2014, **3**, e141; (b) H. Zhu, C. C. Lin, W. Luo, S. Shu, Z. Liu, Y. Liu, J. Kong, E. Ma, Y. Cao, R.-S. Liu and X. Chen, *Nat. Commun*., 2014, **5**, 4312; (c) T. Pulli, T. Donsberg, T. Poikonen, F. Manoocheri, P. Karha and E. Ikonen, *Light*: *Sci*. & *Appl*., 2015, **4**, e332.

3 (a) P. Psuja, D. Hreniak and W. Strek, *J. Nanomater*. 2007, 81350; (b) F. Wang and X. Liu, *Acc. Chem. Res*., 2014, **47**, 1378; (c) H. Wu, L. Ying, W. Yang and Y. Cao, *Chem. Soc. Rev*., 2009, **38**, 3391.

4 (a) S. Nakamura and G. Fasol, The Blue Laser Diode, Springer, Berlin, 1996; (b) Amit K. Vishwakarma, Kaushal Jha, M. Jayasimhadri, B. Sivaiah, Bhasker Gahtoria, and D. Haranath, *Dalton Trans*., 2015, **44**, 17166.

5 (a) Z. Hao, J. Zhang, X. Zhang, X. Sun, Y. Luo, S. Lu and X.-J. Wang, *Appl. Phys. Lett*., 2007, **90**, 261113; (b) C. Liang, H. You, Y. Fu, X. Teng, K. Liu and J. He, *Dalton Trans*., 2015, **44**, 8100.

6 (a) S. Zhang, Y. Nakai, T. Tsuboi, Y. Huang and H. J. Seo, *Inorg. Chem*., 2011, **50**, 2897; (b) W. J. Yang and T. M. Chen, *Appl. Phys. Lett*., 2006, **88**, 101903.

7 (a) B. Yuan, Y. Huang, Y. M. Yu, H. J. Seo, *Ceram. Inter*., 2012, **38**, 2219; (b) R. Yu, S. Zhong, N. Xue, H. Lia and H. Ma, *Dalton Trans*., 2014, **43**, 10969; (c) J. Li, J. Liu, X. Yu, *J. Alloys Compd*., 2011, **509**, 9897.

8 G. Li, Y. Tian, Y. Zhao and J. Lin, *Chem. Soc. Rev*., 2015, **44**, 8688.

9 F. Kang, M. Peng, X. Yang, G. Dong, G. Nie, W. Liang, S. Xu and J. Qiu, *J. Mater. Chem. C*, 2014, **2**, 6068.

10 (a) C. Guo, X. Ding, L. Luan, Y. Xu, *Sensors and Actuators B*, 2010, **143**, 712; (b) M. Xie, D. Li, R. Pan, X. Zhou and G. Zhu, *RSC Adv*., 2015, **5**, 22856; (c) S. Park, Mater. Lett., 2014, 135, 59; (d) S. Lee, S. Park, *J. Lumin*., 2013,**143**, 215; (e) S. C. Gedam, S. J. Dhoble, K. Park, *J. Lumin*., 2013, **139**, 47; (f) I. V. B Maggay, P.-C. Lin and W.-R. Liu, *J. Solid State Lighting*, 2014, **1**, 13; (g) G. Ju, Y. Hu, L. Chen, X. Wang, Z. Mu, H. Wu, F. Kang, *J. Lumin*., 2012, **132**, 1853.

11 (a) A. Li, D. Xu, H. Lin, S. Yang, Y. Shao, Y. Zhang and Z. Chen, *RSC Adv*., 2015, **5**, 45693; (b) M. Xie, G. Zhu, L. Zeng, F. Xie, and C. Liang, *Int. J. Appl. Ceram. Technol*., 2015, **12**, 750.

12 G. Ju, Y. Hu, L. Chen, X. Wang and Z. Mu, *Opt. Mater*., 2014, **36**, 1183.

13 K. Li, D. Chen, J. Xu, R. Zhang, Y. Yu and Y. Wang, *Mater. Res. Bull*., 2014, **49**, 677.

14 V. RaoBandi, B. K. Grandhe, K. Jang, S.-S. Kim, D.-S. Shin, Y.-I. Lee, J.-M. Lim and T. Song, *J. Lumin*., 2011, **131**, 2414.

15 X. Zhang, Z. Lu, F. Meng, F. Lu, L. Hu, X. Xu and C. Tang, *Mater. Lett*., 2012, **66**, 16.

16 M. Krings, G. Montana, R. Dronskowski and C. Wickleder, *Chem. Mater*., 2011, **23**, 1694.

17 P. Pust, V. Weiler, C. Hecht, A. Tücks, A. S. Wochnik, A.-K. Hen, D. Wiechert, C. Scheu, P. J. Schmidt and W. Schnick, *Nat. Mater*., 2014, **13**(9), 891.

18 Z. Tao, Y. Huang and H. J. Seo, *Dalton Trans*., 2013, **42**, 2121.

19 N. Komuro, M. Mikami, Y. Shimomura, E. G. Bithell and A. K. Cheethamd, *J. Mater. Chem. C*, 2015, **3**, 204.

20 X. Gong, J. Huang, Y. Chen, Y. Lin, Z. Luo and Y. Huang, *Inorg. Chem*., 2014, **53**, 6607.

21 J. H. Kim and K. Y. Jung, *J. Lumin*., 2012, **132**, 1376.

22 X. Wang, G. Zhou, H. Zhang, H. Li, Z. Zhang and Z. Sun, *J. Alloys Compd*., 2012, **519**, 149.

23 K. Dagmara, C. Joanna, S. Luis, B. Zoila and Z. Eugeniusz, *J. Phys. Chem. C*, 2015, **119**, 27649.

24 Y. Xia, F. Huang, W. Wang, A. Wang and J. Shi, *J. Alloys Compd*., 2009, **476**, 534.

25 Z. Yang, Z. Zhao, Y. Wen and Y. Wang, *J. Alloys Compd*., 2013, **559**, 142.

26 H. Ju, W. Deng, B. Wang, J. Liu, X. Tao and S. Xu, *J. Alloys Compd*., 2012, **516**, 153.

27 F. Kang, M. Peng, Q. Zhang and J. Qiu, *Chem. Eur. J*., 2014, 20, 11522.

28 F. Kang, Y. Zhang, L. Wondraczek, J. Zhu, X. Yang and M. Peng, *J. Mater. Chem. C*, 2014, **2**, 9850.

29 D. Haranath, S. Mishra, S. Yadav, R. K. Sharma, L. M. Kandpal, N. Vijayan, M. K. Dalai, G. Sehgal and V. Shanker, *Appl. Phys. Lett*., 2012, **101**, 221905.

30 B. Lei, Y. Liu, Z. Ye and C. Shi, J. Lumin., 2004, **109**, 215.

31 J. Lv, F. Du, R. Zhu, Y. Huang and H. J. Seo, *J. Mater. Chem*., 2011, **21**, 16398.

32 X. Zhou, X. Yang, T. Xiao, K. Zhou, T. Chen, H. Yan and Z. Wang, *J. Rare. Earth*, 2013, **31**, 665.

33 Z. Rui and W. Xiang, *J. Alloys Compd*., 2011, **509**, 1197.

34 Z. Zhang, Z. Mao, S. Song, J. Zhang, L. Liu, W. Zhang and D. Wang, *Mater. Lett*., 2013, **90**, 1.

35 Y. Tian, B. Chen, B. Tian, R. Hu, J. Sun, L. Cheng, H. Zhong, X. Li, J. Zhang, Y. Zhen, T. Yu, L. Huang and Q. Meng, *J. Alloys Compd*., 2011, **509**, 6096.

36 X. Lin, X. Qiao and X. Fan, *Solid State Sci*., 2011, **13**, 579.

37 X. Sun, Z. Hao, C. Li, X. He, H. Qi, L. Yu, Y. Luo, J. Zhang, J. Gao and R. Zhong, *J. Lumin*., 2013, **134**, 191.

38 S. Xin, Y. Wang, G. Zhu, X. Ding, W. Geng and Q. Wang, *Dalton Trans*., 2015, **44**, 16099.

39 M. M. Shang, C. X. Li and J. Lin, *Chem. Soc. Rev*., 2014, **43**,

1372.
40 T. Forster, *Ann*. *Physik*, 1948, **2**, 55.
41 D. L. Dexter, *J*. *Chem*. *Phys*., 1953, **21**, 836.
42 (a) R. Pang, C. Li, L. Shi and Q. Su, *J*. *Phys*. *Chem*. Solids., 2009, **70**, 303; (b) M. P. Saradhi and U. V. Varadaraju, *Chem*. *Mater*., 2006, **18**, 5267; (c) M. C. Chang, J. W. Petrich, D. B. McDonald and G. R. Fleming, *J*. *Am*. *Chem*. *Soc*., 1983, **105**, 3819.
43 (a) S. Nakamura, M. Senoh and T. Mukai, *Appl*. *Phys*. *Lett*., 1993, **62**, 2390; (b) L. Wang, X. Zhang, Z. H. Hao, Y. S. Luo, J. H. Zhang and X. J. Wang, *J*. *Appl*. *Phys*., 2010, **108**, 093515.
44 (a) D. L. Dexter and J. A. Schulman, *J*. *Chem*. *Phys*., 1954, **22**, 1063; (b) R. Reisfeld and N. L. Soffer, *J*. *Solid State Chem*., 1979, **28**, 391.
45 (a) W. J. Yang, L. Y. Luo, T. M. Chen and N. S. Wang, *Chem*. *Mater*., 2005, **17**, 3883; (b) G. Zhu, Y. Wang, Z. Ci, B. Liu, Y. Shi and S. Xin, *J*. *Electrochem*. *Soc*., 2011, **158** (8), J236.
46 M. Inokuti and F. Hirayama, *J*. *Chem*. *Phys*., 1965, **43**, 1978.
47 G. Blasse, *Phys*. *Lett*. *A*, 1968, **28**, 444.
48 H. Zhou, Y. Jin, M. Jiang, Q. Wang and X. Jiang, *Dalton Trans*., 2015, **44**, 1102.
49 (a) X. Liu and J. Qiu, *Chem*. *Soc*. *Rev*., 2015, **44**, 8714; (b) K. N. Shinde and S. J. Dhoble, *Critical Reviews in Solid State and Materials Sciences*, 2014, **39**, 459; (c) M. Shang, C. Li and J. Lin, *Chem. Soc. Rev*., 2014,**43**, 1372.
50 L. Liu, L. Wang, C. Zhang, Y. Cho, B. Dierre, N. Hirosaki, T. Sekiguchi and R.-J. Xie, *Inorg*. *Chem*., 2015, **54**, 5556.
51 K. Li, D. Geng, M. Shang, Y. Zhang, H. Lian and J. Lin, *J*. *Phys*. *Chem*. *C*, 2014, **118**, 11026.
52 N. Guo, H. You, C. Jia, R. Ouyang and D. Wu, *Dalton Trans*., 2014, **43**, 12373.
53 Y. Feng, J. Huang, L. Liu, J. Liu and X. Yu, *Dalton Trans*., 2015, **44**, 15006.
54 D. Geng, M. Shang, Y. Zhang, Z. Cheng and J. Lin, E*ur. J. Inorg*. *Chem*., 2013, **16**, 2947.
55 C.-H. Huang, T.-S. Chan, W.-R. Liu, D.-Y. Wang, Y.-C. Chiu, Y.-T. Yeh and T.-M. Chen, *J*. *Mater*. *Chem*., 2012, 22, 20210.
56 (a) P. Li, Z. Wang, Z. Yang and Q. Guo, *J*. *Mater*. *Chem*. *C*, 2014, **2**, 7823; (b) S. Choi, Y. J. Yun and H.-K. Jung, *Mater*. *Lett*., 2012, **75**, 186; (c) M. Guo, L. Huang, S. Zhao, D. Deng, H. Wang, Y. Hua, G. Jia and S. Xu, *J*. *Lumin*., 2013, **134**, 96; (d) N. Guo, Y. Huang, H. You, M. Yang, Y. Song, K. Liu and Y. Zheng, *Inorg*. *Chem*., 2010, **49**, 10907; (e) K. H. Kwon, W. B. Im, H. S. Jang, H. S. Yoo, and D. Y. Jeon, *Inorg*. *Chem*., 2009, **48**, 11525; (f) N. Xie, J. Liu, Y. Huang, S. I. Kim and H. J. Seo, *Ceram*. *Inter*., 2012, **38**, 1489.
57 W.-R. Liu, C.-H. Huang, C.-W. Yeh, J.-C. Tsai, Y.-C. Chiu,Y.-T. Yeh and R.-S. Liu, *Inorg*. *Chem*., 2012, **51**, 9636;
58 Z. Xia, Y. Zhang, M. S. Molokeev and V. V. Atuchin, *J*. *Phys*. *Chem*. *C*, 2013, **117**, 20847.
59 K. Li, M. Xu, J. Fan, M. Shang, H. Lian and J. Lin, *J. Mater. Chem. C,* 2015, **3**, 11618.
60 (a) N. Guo, Y. Huang, M. Yang, Y. Song, Y. Zheng and H. You, *Phys*. *Chem*. *Chem*. *Phys*., 2011, **13**, 15077; (b) N. Guo, Y. Zheng, Y. Jia, H. Qiao and H. You, *J*. *Phys*. *Chem*. *C*, 2012, **116**, 1329.
61 (a) N. Guo, Y. Jia, W. Lü, W. Lv, Qi Zhao, M. Jiao, B. Shao and H. You, *Dalton Trans*., 2013, **42**, 5649; (b) N. Guo, Y. Zheng, Y. Jia, H. Qiao and H. You, *New J. Chem.,* 2012, **36**, 168.
62 Y. Kim and S. Park, *Mater*. *Res*. *Bull*., 2014, **49**, 469.
63 (a) C.-H. Huang, P.-J. Wu, J.-F. Lee and T.-M. Chen, *J*. *Mater*. *Chem*., 2011, **21**, 10489; (b) C.-H. Huang and T.-M. Chen, *Opt*. *Exp*., 2010, **18**, 5089; (c) N. Guo, H. You, Y. Song, M. Yang, K. Liu, Y. Zheng, Y. Huang and H. Zhang, *J*. *Mater*. *Chem*., 2010, **20**, 9061.
64 N. Niu, P. Yang, W. Wang, F. He, S. Gai, D. Wang and J. Lin, *Mater*. *Res*. *Bull*., 2011, **46**, 333.
65 Q. Xu,L. Han, Q. Di and J. Sun, *Ceram*. *Inter*., 2015, **41**, 2699.
66 K. Li, Y. Zhang, X. Li, M. Shang, H. Lian and J. Lin, *Dalton Trans*., 2015, **44**, 4683.
67 M. Jiao, N. Guo, W. Lu, Y. Jia, W. Lv, Q. Zhao, B. Shao and H. You, *Inorg*. *Chem*., 2013, **52**, 10340.
68 M. Zhang, Y. Liang, S. Xu, Y. Zhu, X. Wu and S. Liu, *CrystEngComm*, 2016, **18**, 68.
69 W. Lv, Z. Hao, X. Zhang, Y. Luo, X. Wang and J. Zhang, *Inorg*. *Chem*., 2011, **50**, 7846.
70 L. Jiang, R. Pang, D. Li, W. Sun, Y. Jia, H. Li, J. Fu, C. Li and S. Zhang, *Dalton Trans*., 2015, **44**, 17241.
71 S. Xu, P. Li, Z. Wang, T. Li, Q. Bai, J. Sun and Z. Yang, *J. Mater. Chem. C,* 2015, **3**, 9112.
72 Y. Jia, W. Lv, N. Guo, W. Lv, Q. Zhao and H. You, *Chem. Commun.,* 2013, **49**, 2664.
73 (a) K. Li, M. Shang, H. Lian and J. Lin, *Inorg*. *Chem*., 2015, **54**, 7992; (b) X. Ding, G. Zhu, W. Geng, Q. Wang and Y. Wang, *CrystEngComm*, 2015, 17, 3235; (c) X. Wang and Y. Wang, *J*. Phys. *Chem*. *C*, 2015, **119**, 16208.
74 (a) Y. N. Xue, F. Xiao and Q. Y. Zhang, *Spectrochimica Acta Part A*, 2011, **78** , 1445; (b) B. Zhang, H. Zhong, C. Cai, L.-Y. Hao, X. Xu, S. Agathopoulos and L.-J. Yin, *Mater*. *Res*. *Bull*., 2015, **72**, 83; (c) K. Li, D. Chen, R. Zhang, Y. Yu, J. Xu and Y. Wang, *Mater*. *Res*. *Bull*., 2013, **48**, 1957; (d) M. Shang, G. Li, D. Geng, D. Yang, X. Kang, Y. Zhang, H. Li and J. Lin, *J*. *Phys*. *Chem*. *C*, 2012, **116**, 10222.
75 Y. Zhu, Y. Liang, M. Zhang, M. Tong, G. Li and S. Wang, *RSC Adv*., 2015, **5**, 98350.
76 J. Zhou, T. Wang, X. Yu, D. Zhou and J. Qiu, *Mater*. *Res*. *Bull*., 2016, **73**, 1.
77 Z. Ci, Q. Sun, M. Sun, X. Jiang, S. Qin and Y. Wang, *J*. *Mater*. *Chem*. *C*, 2014, **2**, 5850.
78 (a) D. Wei, Y. Sun, L. Jiang, S. Hua and D. Lia, *New J. Chem.,* 2015, **39**, 4753; (b) W. Lv, W. Lü, N. Guo, Y. Jia, Q. Zhao, M. Jiao, B. Shao and H. You, *Dalton Trans*., 2013, **42**, 13071.
79 D. L. Dexter and J. H. Schulman, *J. Chem. Phys*., 1954, **22**, 1063.
80 (a) X. Zhang, L. Zhou and M. Gong, *ECS J. Solid State Sci*. and Tech., 2013, **2**, R83; (b) J. Sun, Z. Lian, G. Shen and D. Shen, *RSC Adv*., 2013, **3**, 18395.
81 W. Lü, Y. Luo, Z. Hao, X. Zhang, X. Wang and J. Zhang, *Mater*. *Lett*., 2012, **77**, 45.
82 (a) M. Jiao, Y. Jia, W. Lü, W. Lv, Q. Zhao, B. Shao and H. You, *Dalton Trans*., 2014, **43**, 3202; (b) Y. Li, Y. Shi, G. Zhu, Q. Wu, H. Li, X. Wang, Q. Wang and Y. Wang, *Inorg*. *Chem*., 2014, **53**, 7668.
83 Y. Jia, Y. Huang, N. Guo, H. Qiao, Y. Zheng, W. Lv, Q. Zhao and H. You, *RSC Adv*., 2012, **2**, 2678.
84 Y. Liu, X. Zhang, Z. Hao, Y. Luo, X. Wang and J. Zhang, *J*. *Mater*. *Chem*., 2011, **21**, 16379.
85 Y. Liu, X. Zhang, Z. Hao, Y. Luo, X. Wang and J. Zhang, *Chem. Commun.,* 2011, **47**, 10677.
86 (a) B. Han, J. Zhang, P. Li, J. Li, Y. Bian and H. Shi, *Optik*, 2015, **126**, 1851; (b) T.-W. Kuo and T.-M. Chen, *J*. *Electrochem*. *Soc*., 2010, **157**, J216; (c) J. Sun, Y. Sun, J. Zeng and H. Du, *J*. *Phys*. *Chem*. *Solids*, 2013, **74**, 100; (d) T.

Jiang, X. Yu, X. Xu, H. Yu, D. Zhou and J. Qiu, *Mater. Res. Bull.*, 2014, 51, 80; (e) C. Guo, H. Jing and T. Li, *RSC Adv.*, 2012, **2**, 2119; (f) N. Guo, Y. Song, H. You, G. Jia, M. Yang, K. Liu, Y. Zheng, Y. Huang and H. Zhang, *Eur. J. Inorg. Chem.*, 2010, **29**, 4636.

87 (a) Q. Guo, L. Liao, M. S. Molokeev, L. Mei and H. Liu, *Mater. Res. Bull.*, 2015, **72**, 245; (b) Q. Guo, L. Liao and Z. Xia, *J. Lumin.*, 2014, **145**, 65; (c) Y. Wen, Y. Wang, F. Zhang and B. Liu, *Mater. Chem. Phys.*, 2011, **129**, 1171; (d) X. Zhou, Z. Zhang and Y. Wang, *J. Mater. Chem. C,* 2015, **3**, 3676; (e) Q. Guo, L. Liao, L. Mei, H. Liu and Y. Hai, *J. Solid State Chem.*, 2015, **225**, 149; (f) K. Li, M. Shang, D. Geng, H. Lian, Y. Zhang, J. Fan and J. Lin, *Inorg. Chem.*, 2014, **53**, 6743; (g) B. Zhang, H. Zhong, C. Cai, L.-Y. Hao, X. Xua, S. Agathopoulos and L.-J. Yin, *Mater. Res. Bull.*, 2015, **72**, 83; (h) B. Han, J. Zhang and Y. Lv, *J. Am. Ceram. Soc.*, 2013, **96** [1], 179.

88 Z. Xia and W. Wu, *Dalton Trans.*, 2013, **42**, 12989.

89 Y. X. Pan, W. Wang and G. K. Liu, *J. Alloys Compd.*, 2009, **488**, 638.

90 K. Li, D. Chen, R. Zhang, Y. Yu, J. Xu and Y. Wang, *Mater. Res. Bull.*, 2013, **48**, 1957.

91 B. Yuan, Y. Song, Y. Sheng, K. Zheng, X. Zhou, P. Ma, X. Xu and H. Zou, *J. Solid State Chem.*, 2015, **232**, 169.

92 D. Geng, K. Li, H. Lian, M. Shang, Y. Zhang, Z. Wu and J. Lin, *Eur. J. Inorg. Chem.*, 2014, **11**, 1955.

93 (a) M. Xu, L. Wang, D. Jia and L. Liu, *Mater. Res. Bull.*, 2015, **70**, 691; (b) Z. Yang, P. Liu, L. Lv, Y. Zhao, Q. Yu and X. Liang, *J. Alloys Compd.*, 2013, **562**, 176; (c) M. Li, Z. Xia and Z. Wang, *Opt. Mater.*, 2014, **37**, 446; (d) M. Xie, S. Ou, H. Liang, D. Hou, Y. Huang, Z. Gao and Y. Tao, *Mater. Chem. Phys.*, 2013, **142**, 339.

94 L. Zhou, H. Liang, P. A. Tanner, S. Zhang, D. Hou, C. Liu, Y. Tao, Y. Huang and L. Li, *J. Mater. Chem. C*, 2013, **1**, 7155.

95 H. Chen, C. Li, Y. Hua, L. Yu, Q. Jiang, D. Deng, S. Zhao, H. Ma and S. Xu, *Ceram. Inter.*, 2014, **40**, 1979.

96 (a) Y. Jia, H. Qiao, Y. Zheng, N. Guo and H. You, *Phys. Chem. Chem. Phys.,* 2012, **14**, 3537; (b) G. Li, M. Li, L. Li, H. Yu, H. Zou, L. Zou, S. Gan and X. Xu, *Mater. Lett.*, 2011, **65**, 3418; (c) S. Miao, Z. Xia, M. S. Molokeev, J. Zhang and Q. Liu, *J. Mater. Chem. C,* 2015, **3**, 8322; (d) M. Chen, Z. Xia, M. S. Molokeev and Q. Liu, *J. Mater. Chem. C*, 2015, **3**, 12477.

97 (a) Y. Song, G. Jia, M. Yang, Y. Huang, H. You and H. Zhang, *Appl. Phys. Lett.*, 2009, **94**, 091902; (b) Y. Jia, R. Pang, H. Li, W. Sun, J. Fu, L. Jiang, S. Zhang, Q. Su, C. Li and R.-S. Liu, *Dalton Trans.*, 2015, **44**, 11399.

98 (a) G. Li, D. Geng, M. Shang, Y. Zhang, C. Peng, Z. Cheng and J. Lin, *J. Phys. Chem. C,* 2011, **115**, 21882; (b) G. Li, Y. Zhang, D. Geng, M. Shang, C. Peng, Z. Cheng and J. Lin, *ACS Appl. Mater. Interfaces*, 2012, **4**, 296; (c) H. Liu, Y. Luo, Z. Mao, L. Liao and Z. Xia, *J. Mater. Chem. C*, 2014, **2**, 1619.

99 Y. Zhang, G. Li, D. Geng, M. Shang, C. Peng, Z. Cheng and J. Lin, *Inorg. Chem.*, 2012, **51**, 11655.

100 C. Feldman, *Phys. Rev.*, 1960, **117**, 455.

101 (a) K. Li, M. Shang, Y. Zhang, J. Fan, H. Lian and J. Lin, *J. Mater. Chem. C,* 2015, **3**, 7096; (b) D. Geng, M. Shang, Y. Zhang, H. Lian, Z. Cheng and J. Lin, *J. Mater. Chem. C*, 2013, **1**, 2345.

102 (a) X. Zhang and M. Gong, *Dalton Trans.*, 2014, **43**, 2465; (b) J. Zhang , Y. He, Z. Qiu, W. Zhang, W. Zhou, L. Yu and S, Lian, *Dalton Trans.*, 2014, **43**, 18134; (c) Y. Zhang, D. Geng, M. Shang, Y. Wu, X. Li, H. Lian, Z.Cheng and J. Lin, *Eur. J. Inorg. Chem.,* 2013, **25**, 4389; (d) Z. Wang, P. Li, Z. Yang, Q. Guo and G. Dong, *Ceram. Inter.*, 2014, **40**, 15283.

103 (a) G. Blasse and A. Bril, *J. Chem. Phys.*, 1967, **47**, 1920; (b) K. C. Bleijenberg and G. Blasse, *J. Solid State Chem.*, 1979, **28**, 303.

104 D. Wen and J. Shi, *Dalton Trans.*, 2013, **42**, 16621.

105 X. Liu and J. Lin, *J. Mater. Chem.*, 2008, **18**, 221.

106 (a) I. Laulicht and S. Meirman, *J. Lumin.*, 1986, **34**, 287; (b) M. Bettinelli, A. Speghini, F. Piccinelli, J. Ueda and S. Tanabe, *Opt. Mater.*, 2010, **33**, 119.

107 (a) J. Zhou and Z. Xia, *J. Mater. Chem. C,* 2015, **3**, 7552; (b) X. Zhang, L. Zhou, Q. Pang, J. Shi and M. Gong, *J. Phys. Chem. C*, 2014, **118**, 7591; (c) X. Zhang, Y. Chen, L. Zhou, Q. Pang and M. Gong, *Ind. Eng. Chem. Res.*, 2014, **53**, 6694; (d) X. Zhang, L. Zhou, Q. Pang and M. Gong, *Opt. Mater.*, 2014, **36**, 1112.

108 X. Zhang, J. Zhang and M. Gong, *Mater. Lett.*, 2015, **143**, 71.

109 H. Yu, X. Yu, X. Xu, D. Zhou and J. Qiu, *ECS J. Solid State Sci. Tech.*, 2014, **3** (12), R245.

110 (a) S. Yan, J. Zhang, X. Zhang, S. Lu, X. Ren, Z. Nie and X. Wang, *J. Phys. Chem. C*, 2007, **111**, 13256; (b) L. Wan, S. Lv, L. Sun and X. Qu, *Opt. Mater.*, 2014, **36**, 628; (c) P. Du, L. K. Bharat and J. S. Yu, *J. Alloys Coumd.*, 2015, **633**, 37; (d) R. Cao, G. Chen, X. Yu, C. Cao, K. Chen, P. Liu and S. Jiang, *J. Solid State Chem.*, 2014, **220**, 97.

*111* H. Zhou, Q. Wang and Y. Jin, *J. Mater. Chem. C,* 2015, **3**, 11151.

112 (a) K. Li, J. Fan, M. Shang, H. Lian and J. Lin, *J. Mater. Chem. C,* 2015, **3**, 9989; (b) T. Matsunaga, S. Takeshita and T. Isobe, *J. Lumin.*, 2015, **165**, 62; (c) N. Dhananjaya, H. Nagabhushana, B.M. Nagabhushana, S. C. Sharma, B. Rudraswamy, N. Suriyamurthy, C. Shivakumara and R. P. S. Chakradhar, *Appl. Phys. B*, 2012, **107**, 503; (d) H. Zhou, Y. Jin, M. Jiang, Q. Wang and X. Jiang, *Dalton Trans.*, 2015, **44**, 1102.

113 K. Li, H. Lian, M. Shang and J. Lin, *Dalton Trans.*, 2015, **44**, 20542.

114 L. Wang, H. Guo, Y. Wei, H. M. Noh and J. H. Jeong, *Opt. Mater.*, 2015, **42**, 233.

115 C. Zeng, Y. Hu, Z. Xia and H. Huang, *RSC Adv.*, 2015, **5**, 68099.

116 (a) J. Zhou and Z. Xia, *J. Mater. Chem. C*, 2014, **2**, 6978; (b) X. Zhang, L. Zhou, J. Shi and M. Gong, *Mater. Lett.*, 2014, **137**, 32.

117 W. Xie, G. Liu, X. Dong, J. Wang and W. Yu, *RSC Adv.*, 2015, **5**, 77866.

118 (a) H. Liu, L. Liao, J. Chen, Q. Guo, Y. Zhang and L. Mei, *J. Lumin.*, 2016, **169**, 739; (b) T. Wang, X. Xu, D. Zhou, J. Qiu and X. Yu, *J. Rare Earth*, 2015, **33**, 361; (c) Y. I. Jeon, L. K. Bharat and J. S. Yu, *J. Lumin.*, 2015, **166**, 93.

## Graphic Abstract

A series of recent energy transfer phosphors systems with different and controllable emission colors have been summarized in this article.